An HIV-1 Reference Epitranscriptome

Michael S. Bosmeny[1,2], Adrian A. Pater[1,2], Li Zhang[2,3], Beverly E. Sha[4], Zidi Lyu[5], Lydia Larkai[1], Masad J. Damha[5], Joao I. Mamede[3,*], and Keith T. Gagnon[1,*]

[1] Dept. of Biochemistry, Wake Forest University, School of Medicine, Winston-Salem, North Carolina, USA, 27101
[2] Equally contributing authors.
[3] Dept. of Microbial Pathogens and Immunity, Rush University, Chicago, Illinois, USA, 60612
[4] Division of Infectious Diseases, Rush University Medical Center, Chicago, Illinois, USA, 60612
[5] Dept. of Chemistry, McGill University, Montreal, Canada, H3A, 0G3
* To whom correspondence should be addressed: joao_mamede@rush.edu, ktgagnon@wakehealth.edu

ABSTRACT

Post-transcriptional chemical modifications to RNA, or the epitranscriptome, play important roles in RNA metabolism, gene regulation, and human disease, including viral pathogenesis. Modifications to the RNA viral genome and transcripts of human immunodeficiency virus 1 (HIV-1) have been reported, including methylation of adenosine (m^6A) and cytosine (m^5C), acetylation of cytosine, pseudouridylation (psi), and conversion of adenosine to inosine, and their effects on virus and host biology have been investigated. However, diverse experimental approaches have been used, making clear correlations across studies difficult to assess. To address this need, we propose the establishment of a reference HIV-1 epitranscriptome. We sequenced the model NL4-3 HIV-1 genome from infected Jurkat CD4+ T cells cells using the latest nanopore chemistry, custom RNA preparation methods, and commercial base-calling algorithms. This resulted in a reproducible sense and preliminary antisense HIV-1 epitranscriptome where m^6A, m^5C, psi, ands inosine could be identified by multiplexed base-calling. Multiplexed base-calling miscalled modifications due to sequence and neighboring modification contexts, which we demonstrate can be corrected with synthetic HIV-1 RNA fragments. We validate m^6A modification sites with a small molecule inhibitor of methyltransferase-like 3 (METTL3), STM2457. We conclude that modifications do not change substantially under combination antiretroviral therapy (cART) treatment or in primary CD4+ T cells. Samples from patients living with HIV reveal conservation of certain modifications, such as m^6A. Our approach and reference data offer a straightforward benchmark that can be adopted to help advance rigor, reproducibility, and uniformity across future HIV-1 epitranscriptomics studies.

INTRODUCTION

Epitranscriptomics is the study of post-transcriptional RNA chemical modifications and their functional effects on RNA in biology, disease, and beyond (Cerneckis et al., 2024). While epitranscriptomics is an established field of investigation, it is constantly evolving with the characterization of new modifications in unexpected places (Gao et al., 2025; Yan et al., 2025; Zhang et al., 2021), methods to identify them (Cai et al., 2024; Cerneckis et al., 2024; Ron et al., 2025; Roundtree et al., 2017), and pathways they impact in biology and disease (Cerneckis et al., 2024; Jia et al., 2025; Phillips et al., 2024). Nonetheless, experimental and bioinformatic tools like the m^{6}A-Atlas (Liang et al., 2024; Tang et al., 2021) or the MODOMICS database (Boccaletto et al., 2022; Dunin-Horkawicz et al., 2006) can provide useful reference points across studies. Viral RNAs, for example, often possess their own unique epitranscriptomes that can either control viral pathogenesis, such as viral gene expression and replication, or modulate host pathways like the innate immune response (Chen et al., 2021; Phillips et al., 2024; Schultz et al., 2025; Verhamme and Favoreel, 2025).

The RNA modifications of human immunodeficiency virus 1 (HIV-1) represent one of the most well-studied viral epitranscriptomes (Phillips et al., 2024; Wang et al., 2022). Most sequencing-based studies have focused on N^6-methyladenosine (m^{6}A) (Baek et al., 2024; Chen et al., 2021; Lichinchi et al., 2016; Mishra et al., 2024; Pereira-Montecinos et al., 2022; Tirumuru et al., 2016; Tsai et al., 2021). Other modifications, including 5-methylcytosine (m^{5}C) (Courtney et al., 2019; Huang et al., 2023), N^4-acetylcytidine (ac^{4}C) (Tsai et al., 2020), pseudouridine (psi, Ψ) (Martinez Campos et al., 2021), and inosine (Sharmeen et al., 1991) have also been investigated but are less understood. It is currently difficult to establish a clear consensus on the RNA modification landscape of HIV-1, especially beyond m^{6}A, due to the diversity of experimental methods. Several groups have mapped suspected regions for a single modification type at a time, often by an antibody-based method, but these do not have single-nucleotide resolution (Kennedy et al., 2016; Lichinchi et al., 2016; Tirumuru et al., 2016). Other techniques that do have single-nucleotide resolution, such as bisulfite sequencing for m^{5}C detection (Huang et al., 2023) or m^{6}A-SAC-seq for m^{6}A (Mishra et al., 2024), can sometimes be challenging to execute and interpret.

Having a standard approach for identifying HIV-1 RNA modifications that produces consistent results, can be utilized for multiple modifications, is straightforward to implement, and can be

correlated across multiple studies as a benchmark would help advance the field. Here we establish a reference methodology and epitranscriptome for HIV-1 using a common model virus genome, NL4-3, and the model Jurkat T cell line. In addition, two RNA library preparation methods, ribosomal RNA (rRNA) depletion and poly-A selection, are combined to provide more consistent coverage followed by nanopore direct RNA sequencing (dRNA-seq) with the latest flow cell chemistry. The most up-to-date base calling algorithms from Oxford Nanopore Technologies (ONT) are applied for multiplex base-calling of m^6A, m^5C, psi, and inosine. We report substantial miscalling errors with current ONT algorithms due to unique sequence and modification contexts of the HIV-1 viral RNA and provide baseline subtraction and correction methods to address them. This resulted in a refined modification map of the sense and partial antisense epitranscriptomes of HIV-1 that can serve as a reference. We validated m^6A modifications using small molecule inhibition of methyltransferase-like 3 (METTL3) and applied our approach to mapping modifications in Jurkat cells treated with physiological levels of current first-line combination antiretroviral therapy (cART) treatment, primary CD4+ T cells, and CD4+ T cells from people living with HIV-1 (PLWH). Together, these results provide a roadmap and reference for creating HIV-1 epitranscriptomes for high confidence modification calling using state-of-the-art ONT nanopore sequencing.

RESULTS

Direct RNA sequencing provides multiplexed base modification calling on HIV-1 viral RNA

To create an accessible methodology for a reference HIV-1 epitranscriptome, we selected a commonly used NL4-3 HIV-1 genome and model Jurkat T cells. We also selected the Oxford Nanopore Technologies (ONT) nanopore-based direct RNA sequencing (dRNA-seq) platform. Nanopore sequencing is a cost-effective, commercial technology that is well-supported and can perform direct sequencing of RNA with minimal alteration and without amplification (Jain et al., 2022). Importantly, dRNA-seq has been used previously to sequence HIV-1 viral RNAs (Baek et al., 2024; Honeycutt et al., 2024; Li et al., 2024), albeit with older flow cell technologies and limited baseline correction. However, ongoing improvements in flow cell chemistry, as well as bioinformatic base-calling tools, have made dRNA-seq an increasingly attractive off-the-shelf solution for multiplexed identification of RNA modifications. The combination of these model

systems offers an opportunity to establish a benchmark method and data set that is robust, reproducible, and accessible to help advance HIV-1 epitranscriptomics studies.

Our standard approach was to infect Jurkat cells with non-replicative HIV-GFPΔEnv/VSV-G virus, which contains a partial replacement of the *nef* gene with GFP that also induces a frameshift in the *env* gene (hereafter referred to as NL4-3-GFP). Total RNA was collected and depleted of rRNA, poly-A selected, or both. The enriched RNA was directly sequenced on an ONT PromethION system. We performed base-calling with ONT algorithms to calculate likely modification sites for m^6A, m^5C, pseudouridine, and inosine. Initial experiments were performed in three biological replicates and demonstrated high reproducibility across the NL4-3-GFP HIV-1 genome (**Figure S1**). To validate modifications, we treated Jurkat cells with STM2457 at the time of infection. STM2457 is an inhibitor of catalysis for METTL3 (Yankova et al., 2021), the primary methyltransferase that writes m^6A onto RNA. A 30 μM dose of STM2457 was sufficient to reduce detection of all m^6A modification sites on NL4-3-GFP RNA to less than half their normal value, on average (**Figure 1A**). This result supported accurate m^6A identification by the current ONT algorithm.

Background subtraction and correction of HIV-1 modification calls

In our initial data set, an interesting modification pattern was consistently observed at the 3' end of the HIV-1 transcript, where the majority of m^6A sites are predicted. METTL3 conversion to m^6A strongly prefers a DRACH motif (A/U/G, A/G, A, C, A/U/C). The m^6A modification itself occurs at the central adenosine, which is always followed by cytosine and then often uridine. Several of these m^6A modification locations were reported by the base-calling algorithm to also possess substantial amounts of m^5C followed by psi in an ACU motif (**Figure 1B**). One possible explanation for such a modification pattern would be miscalling due to sequence motif context or nearby modifications influencing the base-calling of others. Nanopore sequencing reads nucleic acids in five-nucleotide 'frames,' or k-mers, that shift one base at a time to generate current signals. This can lead to modification calling artifacts, especially for uncommon sequence motifs or unaccounted nucleotide modifications, during computational interpretation of current signals. Unexpectedly, treatment with STM2457 not only reduced the m^6A at these ACU motifs, but also the m^5C, suggesting a dependence on m^6A presence (**Figure 1B**). Conversely, the psi calls in these

ACU motifs did not respond to STM2457 treatment. Thus, we questioned the legitimacy of m^5C in these ACU motifs.

To better understand m^5C calls in ACU motifs, we synthesized RNA oligonucleotides bearing the two adjacent ACU motifs found in the NL4-3-GFP genome where m^6A is called at positions 8975 and 8989. One oligonucleotide contained no modifications while the other contained m^6A at both positions. When these oligonucleotides were sequenced, we observed substantial m^5C calling in the ACU motifs only when m^6A was present (**Figure 1C-E**). These results clearly identified the presence of m^6A as a modifier that induces false positive m^5C calls within these motifs. Interestingly, psi was observed at significant levels in unmodified RNA in the absence of m^6A, as was m^5C to a lesser extent, at certain nucleotides, indicating background calling due to sequence context (**Figure 1D**).

To address the potential influence of sequence motifs on modification calling at a broader scale, we prepared overlapping multi-kilobase DNA templates from an NL4-3 plasmid (replicative variant without GFP) for *in vitro* T7 RNA polymerase transcription. Fragments were *in vitro* transcribed and sequenced, revealing very minimal background miscalling for m^6A, low miscalling for inosine, and more substantial sequence-dependent miscalling for m^5C and psi (**Figure S2**). Using the modification calling frequencies from *in vitro* transcribed NL4-3 fragments, we performed a baseline correction (Baek et al., 2024). After correction, original calling of m^6A remained nearly unchanged, indicating that the base-calling algorithm is likely quite accurate (**Figure 2A, Table S1**). In contrast, only a handful of high-confidence calls for m^5C, psi, and inosine modifications were observed across the NL4-3-GFP viral RNAs after correction (**Figure 2B-D, Tables S2-S4**). This method of baseline correction should be applicable to many defined sequences, especially smaller viral transcriptomes of limited size.

Features of the corrected HIV-1 epitranscriptome

Several observations can be noted for the different modifications identified in NL4-3-GFP viral RNAs. For m^6A, nearly all high-frequency modifications are found on the 3' end of the genome, in approximately the last thousand bases (**Figure 2A**). These include a pair at positions 8079 and 8110, which occur in the region where *rev* and *env* genes overlap, and a trio at 8947, 8975, and 8989 in the 3' LTR just beyond the end of the *nef* gene. Evidence for m^6A modifications in these

areas is well-documented, with previous MeRip-Seq and PA-m^{6}A-Seq experiments showing high probabilities of m^{6}A in these regions (Courtney et al., 2019; Kennedy et al., 2017; Lichinchi et al., 2016; Pereira-Montecinos et al., 2022; Tirumuru et al., 2016). One group used silent mutations to remove individual A nucleotides at each position or all three together (A8079G, A8975C, and A8989T) (Baek et al., 2024). The triple mutation resulted in reduced HIV-1 protein expression. There is also a trio of m^{6}A modifications in the middle of the *nef* gene (8571, 8621, and 8710), but these methylations may be artificially induced. The NL4-3-GFP genome possesses a GFP tag that replaces approximately the first one hundred bases of the *nef* gene (**Table S1**) and the frequency of these modifications are dramatically reduced when a non-GFP genome is used, which we describe later. Finally, there is a single m^{6}A modification (3108) that is present in the middle of the *pol* gene. While it does not exhibit a high level of modification, it is notable for being the only significant m^{6}A not on the 3' end of the genome. A previous study suggested an m^{6}A in this region but lacked single-nucleotide resolution (Cristinelli et al., 2021).

After baseline correction, only a few m^{5}C modifications emerged (**Figure 2B**). Position 8514, in the *nef* gene, is perhaps the most consistent m^{5}C-called position. All samples indicated m^{5}C frequencies ranging from 65-75% at this position (**Table S2**). Position 2547 in the *env* gene, in contrast, varies widely between samples and exhibits a high background. Positions 547 and 4305, both in the *pol* gene, also have a high degree of variance but with low background. Variability between samples suggests the possibility that these sites are more sensitive to cellular signals.

The ONT base-calling algorithm identified a large number of potential psi modifications when uncorrected (**Figure S1**). However, most of these were also called in the unmodified *in vitro* transcribed viral genome fragments (**Figure S2**), indicating they are likely to be miscalled. After removing background calls, the number of psi decreases dramatically (**Figure 1B** and **2C**). As a general trend, most of the psi called in NL4-3-GFP are in runs of multiple uridines (**Figure S2C inset**). However, not every modification site is in a cluster, and not every cluster has a psi call, indicating nuances in sequence context. Like m^{5}C, there is higher variance in psi at a given site from sample to sample, but samples from the same growth date are generally quite similar. For example, site 9171, in the 3' LTR, has high amounts of psi in samples 7C and 7E (25% and 31%, respectively), but lower amounts in 11E, 11B/H, 11F, and 11C/I (3%, 7%, 8%, and 7%, respectively). The six most likely candidates for psi all exhibit this variation (**Table S3**).

The inosine results from the ONT modification-calling algorithm (**Figure 1D**) are the least clear. Even prior to background subtraction, inosine modifications were not called very frequently. Most sites ranged between 10-20% modification. After background subtraction, only a handful of nucleotide positions reached a 10% threshold. This would suggest that inosine may only be present on the HIV-1 sense transcript in low abundance. Given this caveat, the highest frequency inosine modifications were 448 (*gag*), 495 (*gag*), 3088 (*pol*), 3647 (*pol*), 4340 (*pol*), 7966 (*env*), 8037 (*env*), and 8568 (*nef*) (**Table S4**).

RNA preparation methods do not alter modification calling

During sample preparation, two methods of RNA enrichment were performed, a bead-based poly-A selection method and an RNase H-based ribosomal RNA (rRNA) degradation method. Each method yielded a different configuration of RNA fragments for sequencing, allowing a greater diversity of reads. Poly-A selection produced relatively long reads from dRNA-seq that usually began at the 3' end of the viral genome, resulting in high 3' end coverage but low coverage across the middle and 5' end (**Figure S3A**). On the other hand, rRNA depletion resulted in smaller RNA fragments that were well-distributed across the NL4-3-GFP genome (**Figure S3A**). However, poly-A selection alone does not capture host non-coding RNAs efficiently while rRNA depletion on the other hand does not cover protein coding mRNAs well (**Figure S3B**). By combining both methods experimentally, either before or after sequencing, coverage across viral and host transcriptomes can be optimized.

There is the possibility that each of these selection methods could result in modification calling bias due to RNA species enrichment. Therefore, we compared modified base calling between these two methods. Sample 11B/H was prepared in each depletion method separately and each preparation was then sequenced separately. The 3' end of the HIV-1 genome was compared for modifications, as this region received reasonable coverage under both methods. Our analysis shows little difference between methods when calling modifications for HIV-1 (**Figure S3C**). Using only one RNA preparation method should not significantly alter modification calling results for HIV-1 at most positions.

cART treatment does not alter the HIV-1 epitranscriptome

We also wanted to examine the effect of combination antiretroviral therapy (cART) in our model system. Three replicates of Jurkat cells, infected with NL4-3-GFP virions, were treated with

cART prior to RNA collection. These samples were processed and sequenced as before. We observed no obvious differences in modification calling between samples with and without cART treatment (**Figure 3A**). This suggests that cART does not perturb the enzymatic modification pathways in these cells and is not an obvious modifier of the HIV-1 epitranscriptome.

The HIV-1 epitranscriptome in CD4+ T cells from people living with HIV

To assess the epitranscriptome of HIV-1 derived from people living with HIV (PLWH), we first performed sequencing of HIV-1 viral RNA from primary CD4+ T cells, which were isolated from the blood of healthy plasma donors. CD4+ T cells were activated and subsequently infected with a concentrated HIV-1 virus derived from the NL4-3 plasmid, a replicative virus lacking GFP. We then harvested CD4+ T cells from blood plasma of two PLWH patients. RNA was extracted and subjected to dRNA-seq for modification calling. The significantly lower amount of HIV-1 viral RNA in these samples required greater sequencing depth. While full HIV-1 genome coverage was obtained from CD4+ T cells grown and infected in cell culture, we could only obtain 3' end genome coverage for PLWH samples. For modifications where we obtained sufficient coverage from PLWH samples, we compared their levels to that of Jurkat and CD4+ T cells grown in culture (**Figure 3B**). In general, modifications were found at the same positions and at similar frequencies compared to Jurkat cell culture samples. Notably, however, m^6A modifications in CD4+ T cells were called at a lower frequency at nearly all positions. In contrast, m^5C, psi, and inosine frequencies remained approximately the same, albeit at lower frequencies on average.

We noted that m^6A at positions 8564, 8571, 8621, and 8710 were markedly lower for $CD4^+$ T cells as compared to Jurkat samples. The most likely explanation for this discrepancy is the presence of altered sequence, specifically partial replacement of *nef* with GFP, in the NL4-3-GFP genome. This modification may affect RNA folding or otherwise enhance METTL3 recognition. However, when comparing the predicted secondary structure folding of this region, 8571 and 8621 are observed to fall within a hairpin structure that is not expected to change due to the neighboring GFP sequence (**Figure S4**). Overall, samples from different HIV-1 viral RNA sources, including PLWH samples, showed high similarity in modification patterns (**Figure 3B**). This highlights the utility of a reference epitranscriptome across sample types.

The conservation of m^6A modifications, as well as the DRACH motifs where they occur, may hold functional significance. One consideration is the rate of mutation at these sites as compared

to other nucleotide positions across the HIV-1 genome since HIV-1 is known to have a high mutation rate, one of the reasons why developing treatments is complicated (Yeo et al., 2020). Modification position data was compared against two different data sources for wild-type HIV-1 virus sequences: PLWH samples we sequenced and the Nextclade database of reference HIV-1 sequences. For PLWH sequences, the integrity of DRACH motifs at the 3' end of the genome, where most m^6A modifications were confidently called, was compared to the average m^6A frequencies in our reference epitranscriptome (**Figure 3C**). Between HIV-1 genomic positions 8000 and 9172, there are twenty-six DRACH motifs. Of these, twenty were not mutated in either sample. This includes nine high-frequency m^6A modification sites. Of the remaining six DRACH motif sites that were disrupted in one or both PLWH samples, none showed an m^6A modification frequency over 10% in our reference epitranscriptome. We next compared against the Nextclade HIV-1 (HXB2) dataset, which comprises nucleotide diversity of approximately one thousand HIV-1 genomes (Aksamentov et al., 2021). If, for a given nucleotide position, one of the thousand HIV-1 genomes had a mutation, that is counted as one 'event.' Positions with a high mutation frequency would be expected to have a higher number of events. A typical nucleotide position will have approximately fifty events. The highest number of mutation events at any nucleotide position was 406. In contrast, the lowest number of mutation events (1-5 events) were associated with essential genetic components, such as the start codons for HIV-1 proteins. When surveying the nine high-frequency m^6A sites, the average number of events was 16.38, between 10% to 35% of the typical nucleotide mutation rate (**Figure 3C**). Together, these results suggest that these residues may be conserved for their m^6A modification status and therefore play important roles in virus function and fitness.

A novel HIV-1 antisense epitranscriptome

All the above-mentioned modification sites are from RNA in the sense direction. Nanopore dRNA-seq and analysis also enables differentiation of antisense HIV-1 reads, which might allow for modification calling on antisense transcripts, such as those utilized by the *asp* gene. However, antisense transcripts are very low in abundance, especially outside of the *asp* gene. To interrogate the antisense genome, we bioinformatically combined antisense reads from ten Jurkat cell samples. This produced coverage ranging from 10X to 50X across the HIV-1 antisense transcriptome. Because these reads have lower coverage and are combined from multiple samples, results may be intrinsically more variable and should be considered preliminary. To reduce the background noise,

we performed correction with unmodified *in vitro* transcribed RNA fragments and only considered modification calling when at least 10x coverage was present with a calling frequency of >20% (**Table S5**). However, modifications called within the *asp* gene (positions 6910 – 7479) were set to a lower cutoff of 10% frequency due to higher average coverage, its gene status, and previous investigation of this transcripts modifications (Estevez et al., 2022). Interestingly, there were no m^6A calls >20% frequency in the antisense epitranscriptome and only one at just under 20% in the *asp* gene (**Figure 3D**). Conversely, inosine modifications, which were never called above 20% in the sense epitranscriptome, occur at multiple positions in the antisense direction with modification frequencies between 30% and 50%. The highest frequency modification of these inosine sites is position 2680, with 46% of reads called as modified (**Table S4**). There is also one prominent antisense psi called at position 1093 that exhibited no background calling and is called as modified in nearly 70% of reads. Within the *asp* gene itself, the most prominent modification is psi at 7061 (**Figure 3D** and **Table S4**). All four modifications that can be currently called with ONT algorithms, m^6A, m^5C, psi, and inosine, were previously identified by mass spectrometry at low or moderate abundance in *asp* gene antisense transcripts (Estevez et al., 2022). Modifications to the antisense transcripts have not been previously site-specifically mapped and may play a role in the processing or function of the HIV-1 antisense transcriptome.

DISCUSSION

The role of chemical modifications to HIV-1 viral RNA in biology and disease, now referred to as epitranscriptomics, has been a growing topic of investigation for over three decades (Braddock et al., 1991; Sharmeen et al., 1991). Sequencing-based methodologies to both identify the types and map the locations of modifications has significantly improved our understanding of their potential roles (Courtney, 2021; Imam et al., 2020; Phillips et al., 2024; Wang et al., 2022). These findings should enable sequence-specific manipulation of modifications for mechanistic studies as well as potential therapeutic strategies (Abudayyeh et al., 2019; Baek et al., 2024; Chen et al., 2019; Cox et al., 2017; Latifi et al., 2023; Reautschnig et al., 2024; Wilson et al., 2020; Xia et al., 2021; Zhang et al., 2024). Unfortunately, the diversity of sequencing-based methods, among other variables, has made it difficult to correlate findings across multiple studies. Standard inclusion of a common experimental or bioinformatic control would allow for straightforward

normalization and correlation across many studies, providing a standard reference to benchmark against. Such a reference epitranscriptome could help ensure that results were reproducible, rigorous, and well-controlled and advance the study of HIV-1 epitranscriptomics by providing some level of ground truth.

Here, we sought to establish an HIV-1 reference epitranscriptome to strengthen data interpretation, better integrate results with those of other research groups, and create a foundation that the HIV-1 epitranscriptomics community could build upon. Commercial nanopore dRNA-seq reagents, workflows, and bioinformatic tools are broadly accessible and have undergone significant improvements. Thus, nanopore can provide a common tool and dRNA-seq results a common reference for detection of RNA modifications on HIV-1 viral RNAs. Existing data can often be simply reanalyzed when new algorithms become available, making it possible to map new modifications by simply repeating base-calling analyses. In addition, current algorithms enable the equivalent of multiplexed modified base-calling. Together, these features make nanopore-based sequencing for epitranscriptomics cost-effective and data-rich. When combined with commonly used reagents and resources, we found we were able to generate reference methods and data sets that should be broadly useful.

In exploring the potential for an HIV-1 reference epitranscriptome, we used a small molecule inhibitor and synthetic HIV-1 RNA fragments to validate modifications and address miscalling errors. Our miscalling correction approach should be applicable as a general tool and our dRNA-seq data set for subtracting background should apply to all NL4-3 genomes and be helpful in future algorithm retraining. It is important to note that the effects of one modification on the calling of a different modification are complicated and difficult to anticipate. Resolving and refining modification-induced miscalling will likely require careful combinatorial reference data sets to fully address. We also compared efficient RNA preparation techniques, compared effects of cART, and characterized modifications in HIV-1 viral RNA samples from PLWH. We also constructed the first HIV-1 genome-wide antisense epitranscriptome, which could provide unexpected insight into poorly understood HIV-1 antisense transcript biology. As ONT modified base-calling algorithms evolve, these data sets can be reevaluated for continual refining of HIV-1 sense and antisense reference epitranscriptomes.

We found that nanopore-based dRNA-seq was generally robust and reproducible across replicates, cell types, and time. Results in Jurkat cells were quite similar to primary CD4+ T cells. We discovered chemical modification features that have not been previously observed, such as the depletion of m^6A but enrichment of inosine and psi on antisense HIV-1 viral RNAs, which appears to be the inverse for sense viral RNAs. We also discovered m^6A and other modifications, albeit at a lower frequency, on HIV-1 viral RNAs from PLWH. These appear to be conserved across NL4-3 and naturally circulating genomes, though their frequency at individual nucleotide positions may reflect cellular and environmental contexts. Interestingly, treatment with cART had no effect on modifications called at high confidence, suggesting that these drugs do not significantly alter the recognition and modification of HIV-1 RNAs.

Our results provide some implications for individual modifications in HIV-1 viral RNA. While the presence of m^5C was previously reported by Cullen and colleagues using an antibody capture approach (Courtney et al., 2019), another group was unable to detect the same m^5C by bisulfite sequencing methods (Huang et al., 2023). Our results suggest that m^5C is present but at relatively low levels at only a handful of positions, possibly offering an explanation to the two conflicting reports. The m^5C, pseudouridine, and inosine sites that remain at sufficiently high frequency after baseline correction may be worth further investigation. They are relatively distant from other modifications, suggesting they are not miscalled as a result of neighboring modifications, at least for those currently detectable by ONT algorithms. The high accuracy and precision of m^6A calling we observed here, combined with apparent conservation in naturally circulating HIV-1 strains, strengthens the functional significance of m^6A in HIV-1 infection, host innate immunity, replication, and gene expression (Courtney, 2021; Imam et al., 2020; Phillips et al., 2024; Wang et al., 2022).

METHODS

Viral production and quantification

All HIV-1 isolates were generated by transfecting HEK 293T cells using polyethylenimine (PEI; PolySciences). Briefly, for a 10 cm plate production of VSV-G pseudotypes with GFP reporter genes, we mixed 6 µg of HIV-GFPΔEnv and 4 µg of pCMV-VSV-G (gifts from Dr. Thomas J. Hope) as described previously (Mamede et al., 2017), and for replicative HIV-1 pNL4-

3 we used 6 µg pNL4-3 (HIV repository) with 1 mL of opti-MEM (life technologies). 40 µl of PEI was added to the mix, briefly vortexed, and allowed to incubate for 15 min before addition to HEK 293T cells. After overnight transfection, media was changed to fresh DMEM with 10% fetal bovine serum (FBS), 1x penicillin-streptomycin (P/S), and harvested at 48 h post-transfection through a 0.45 µm PVDF membrane filter. For replicative NL4-3, we concentrated the supernatants over a 20% sucrose cushion at 5600 x g overnight in 15 mL tubes. p24 ELISA was performed to quantify the viral preparations (R&D Systems HIV-1 Gag p24 Quantikine ELISA Kit).

Jurkat cell growth and infection

Jurkat (HIV repository) were cultured in RPMI-1640 medium supplemented with 10% FBS, 1x P/S, and non-essential amino acids (NEAA). Cells were split to 2 x 10^5 cells/mL and split when they reached 1.5 x 10^6 cells/mL. When infecting with replicative NL4-3 and pHIVdEnv-GFP, we used a high cell density of ~2.5 x 10^6 cells/mL with a working concentration of HIV p24 (determined by ELISA) of 500-600 ng/mL. Cells were harvested at 45-48 h post-infection and Trizol added at 1mL per 1 x 10^7 cells.

CD4+ T cell negative selection, activation, growth, and infection

In whole blood tubes from unidentified healthy donors or leukopaks (Red Cross Blood) we performed negative cell separation following the vendors protocol with EasySep Direct Human CD4+ T cell Isolation Kits or RosetteSep Human CD4+ T cell Enrichment Cocktail (Stem cell technologies) with Lymphoprep (Stem cell technologies) as density medium f, respectively. Before infection, we activated T cells by adding anti-CD3 and anti-CD28 antibodies along with IL-2 following the methods described previously (Mamede et al., 2017). Activation was confirmed 3 days post-treatment by measuring CD4+/CD69+ double-positive cell percentage by flow cytometry. Briefly: Day 0, isolate CD4+ T cells from blood and activate T cells; Day 3: test activation % and infect CD4+ T cells with WT-HIV. Day 4: TRIUMEQ cART treatment when applicable; Day 6: harvest CD4+ T cells for Trizol lysis as well as quantify infection rate by flow cytometry with KC57 antibody (as described below).

Patient sample $CD4^+$ T cell collection, preparation, and latency reversal

Approximately 10 tubes of whole blood were collected in Heparin tubes typically totaling 85 mL of whole blood. CD4+ T cells were negatively selected with RosetteSep Human CD4+ T cell

Enrichment Cocktail (Stem cell technologies) and SepMate tubes with Lymphoprep (Stem cell technologies) as density medium following the vendor protocol. Cells were activated with anti-CD3 and anti-CD28 antibodies as described above for 3 days. At day 3 cells were fixed for flow cytometry to quantify the percentage of positive p24 cells as described below. The serum on top of the gradient media after centrifugation was collected. Viral particles were concentrated by ultracentrifugation with a 20% sucrose cushion in PBS for 4 h at ~120,000 x g using an SW28 rotor (Beckman Coulter). After concentration, the supernatant was discarded and Trizol was added to the viral pellets (2 mL total for the initial ~85 mL of plasma).

Drug treatments

cART treatment: To model current therapy we added TRIUMEQ with the respective concentrations for each of the antiretrovirals based on reported plasma levels: *ABC 140 ng/mL, 3TC 670 ng/mL, DTG 3.9 ug/mL* (Best et al., 2011; Letendre et al., 2014; McDowell et al., 1999; Mueller et al., 1998; Tashima et al., 1999; van Praag et al., 2002). STM2457 Treatment: STM2457 (MedChemExpress) stocks were dissolved in DMSO and the drug was added simultaneously to infection of NL4-3 at 30 µM or otherwise noted.

Flow cytometry

Flow cytometry was performed with BD CytoFix/Cytoperm per vendor protocol with the following antibodies: To measure activation, anti-CD69 (Fisher Scientific BDB560968) and anti-CD25; and to measure Gag/p24 in the cytoplasm to report infection or viral production, KC57-RD1 (Beckman Coulter, Cat#6604667) antibody (or isotype). Samples were analyzed in a LSRFortessa (BD Biosciences) gating for doublets with SSC-H/SSC-W and FSC-H/FSC-W gates.

RNA extraction and preparation

Total RNA was extracted from cell pellets using standard Trizol protocol. Ribosomal RNA was removed by enzymatic rRNA depletion or poly-A RNA was selected by bead-based enrichment. For rRNA depletion, approximately 20 µg of total RNA was hybridized with DNA oligonucleotides complementary to rRNA (Baldwin et al., 2021). The solution was heated to 95°C and slow cooled to 65°C to oligonucleotide hybridization. Next, RNase H (McLabs, HTRH-200) was added and the solution incubated at 65°C for 5 min to degrade rRNA. DNA was then degraded

using Turbo DNase (Invitrogen, AM2239) and at 37°C for 20 min. RNA was then purified using AMPure XP beads, typically yielding approximately 1000 ng of recovered RNA.

For poly-A selection, the NEBNext High Input Poly(A) mRNA Isolation Module (E3370S) was used following the manufacturer's recommended protocol. Briefly, approximately 20 µg of total RNA was added to a solution containing poly-A-binding beads. After several wash steps, the bead-bound RNA is eluted by heating, typically yielding approximately 500 ng of recovered RNA.

Synthetic and *in vitro* transcribed HIV-1 RNA fragments

For small unmodified and m^6A-modified RNA fragments, 60 nucleotide RNAs were prepared by solid-phase chemical synthesis, HPLC purification, and mass spectrometry confirmation following previously published methods (Ageely et al., 2021; Lackey et al., 2009). Commercially available m^6A phosphoramidite was used (Glen Research). For *in vitro* transcription, pNL4-3 HIV-1 sequence was used to create primers for overlapping amplicons that span the HIV-1 genome. Primers were created with or without a 5' T7 promoter sequence. PCR amplification resulted in T7 promoter-containing fragments of the genome of 2-3 kb size, which were then used as templates in T7 RNA polymerase transcription reactions to make either sense or antisense RNA HIV-1 fragments. Briefly, approximately 1 µg of template DNA was used in a 60 µL reaction following previously published conditions and enzyme preparations (Kartje et al., 2021). Reactions were incubated at 37°C for 90 min then treated with DNase for an additional 20 min at 37°C. RNA was purified by phenol/chloroform extraction and ethanol precipitation. The resulting RNA fragments were combined and sequenced by nanopore in the same manner as cell-derived RNA. Modified base calling was also performed the same as for cell-derived RNA.

Nanopore direct RNA sequencing

For rRNA-depleted samples, polyadenylation reactions were performed using *E. coli* Poly(A) Polymerase (New England Biolabs, M0276L). Briefly, 1000 ng of rRNA-depleted RNA was treated with 0.375 U/µL *E. coli* Poly(A) Polymerase in 1x *E. coli* Poly(A) Polymerase Buffer and 1 mM ATP. The reaction was incubated at 37°C for 2 min and stopped by addition of EDTA to a final concentration of 10mM. The reaction was bead-cleaned using 2x RNAClean XP Beads (Beckman Coulter), washed twice with 200 µL of 75% ethanol, and eluted in 10 µL nuclease-free water. The concentration was determined using the Qubit RNA HS Kit (ThermoFisher Scientific).

Library preparation of the RNA samples was completed using the direct RNA sequencing kit (SQK-RNA004; Oxford Nanopore Technologies, ONT), following manufacturer's recommended protocol. Briefly, RNA samples were quantified using Qubit RNA HS Kit (ThermoFisher Scientific). The RT Adapter was ligated by adding 3 µL of 5x Quick Ligation Buffer (New England Biolabs, NEB), 2 µL of T4 DNA ligase at 2M U/mL (NEB), 1 µL SUPERase·In RNase Inhibitor (20 U/µL) (ThermoFisher Scientific) and incubated at room temperature for 15 min. Reverse transcription was performed using a master mix containing 1x First-Strand Buffer, 10 mM DTT, 0.5 mM dNTPs, and nuclease-free water. The master mix was added to the RT adapter-ligated RNA, followed by the addition of SuperScript III Reverse Transcriptase (ThermoFisher Scientific). Reactions were incubated in a thermal cycler at 50°C for 60 minutes, and 70°C for 10 minutes, with a final hold at 4°C. The reaction was purified using 1.8x RNAClean XP beads (Beckman Coulter), washed twice with 75% ethanol and eluted in 20 µL nuclease-free water. RNA adapter (RMX) ligation was performed by mixing 20 µL of the reverse transcribed RNA, 1x NEBNext Quick Ligation Buffer, 6 µL RNA Adapter (RLA), 3 µL nuclease-free water, and 3 µL T4 DNA Ligase at 2M U/mL (NEB). The mixture was incubated at room temperature for 15 minutes. The reaction was purified using 0.4x RNAClean XP beads (Beckman Coulter), washed twice with Wash Buffer (WSH) and eluted in 33 µL RNA elution buffer (REB). The final library was loaded on a PromethION RNA flow cell (FLO-PRO004RA) and sequenced on a PromethION P2 solo using MinKNOW (v. 24.06.10) with POD5 and live base-calling on. Coverage was monitored using RAMPART software (https://artic.network/rampart), with a goal of 50x coverage across the HIV-1 genome.

Modification calling from Nanopore POD5 files

After the completion of sequencing, reads were called from the POD5 files with Dorado software (v0.8.0) with settings for RNA modifications (RNA basecalling model rna004_130bps_sup@v5.1.0, https://github.com/nanoporetech/dorado). Generated reads were automatically aligned against a FASTA file containing human (hg38) and HIV-1 genomes (https://www.ncbi.nlm.nih.gov/nuccore/AF324493), generating a BAM file.

```
Dorado basecaller sup,m5C,inosine_m6A,pseU [pod5_folder_location]
-b 408 --min-qscore 8 --device cuda:all --reference
[reference_fasta_location] > unsorted_reads.bam
```

After generation of the BAM file, samtools was used to sort and index the BAM file.

```
samtools sort unsorted_reads.bam > sorted_reads.bam

samtools index sorted_reads.bam
```

This sorted BAM file was then processed by modkit (https://github.com/nanoporetech/modkit) to generate a file containing modification sites on the HIV-1 genome. A filter-threshold of 0.7 was utilized to standardize results between runs.

```
   modkit pileup [location_of_BAM] --ref [loc_of_reference] -t 18 --
region NL43_AF324493.2_R2R --max-depth 10000000 --bedgraph ./ --filter-
threshold .7 --motif DRACH 2 --prefix m6A

   modkit pileup [location_of_BAM] --ref [loc_of_reference] -t 18 --
region NL43_AF324493.2_R2R --max-depth 10000000 --bedgraph ./ --filter-
threshold .7 --motif C 0 --prefix m5C

   modkit pileup [location_of_BAM] --ref [loc_of_reference] -t 18 --
region NL43_AF324493.2_R2R --max-depth 10000000 --bedgraph ./ --filter-
threshold .7 --motif T 0 --prefix Psi

   modkit pileup [location_of_BAM] --ref [loc_of_reference] -t 18 --
region NL43_AF324493.2_R2R --max-depth 10000000 --bedgraph ./ --filter-
threshold .7 --motif A 0 --prefix Ino
```

The result is a bedgraph file containing the reference genome name, the position of the calculated modification, the percentage of reads that had the modification, and the total number of reads in the BAM file at that nucleotide position, e.g.:

```
NL43_AF324493.2_R2R        8988   8989   0.64912283   57
```

To remove noise from low-coverage nucleotides, a filter was applied to the bedgraph file, removing modification locations that had less than 10x coverage for that nucleotide position.

```
awk '$5>9' m6A_original.bedgraph > m6A_10xFilter.bedgraph
```

The resulting bedgraph file can be viewed in IGV (https://igv.org/) or opened directly in text-editing software as a tab-separated value (TSV) file.

ACKNOWLEDGEMENTS

This project was funded by a National Institutes of Allergy and Infectious Diseases grant (5R61AI169661) to K.T.G. and J.I.M.

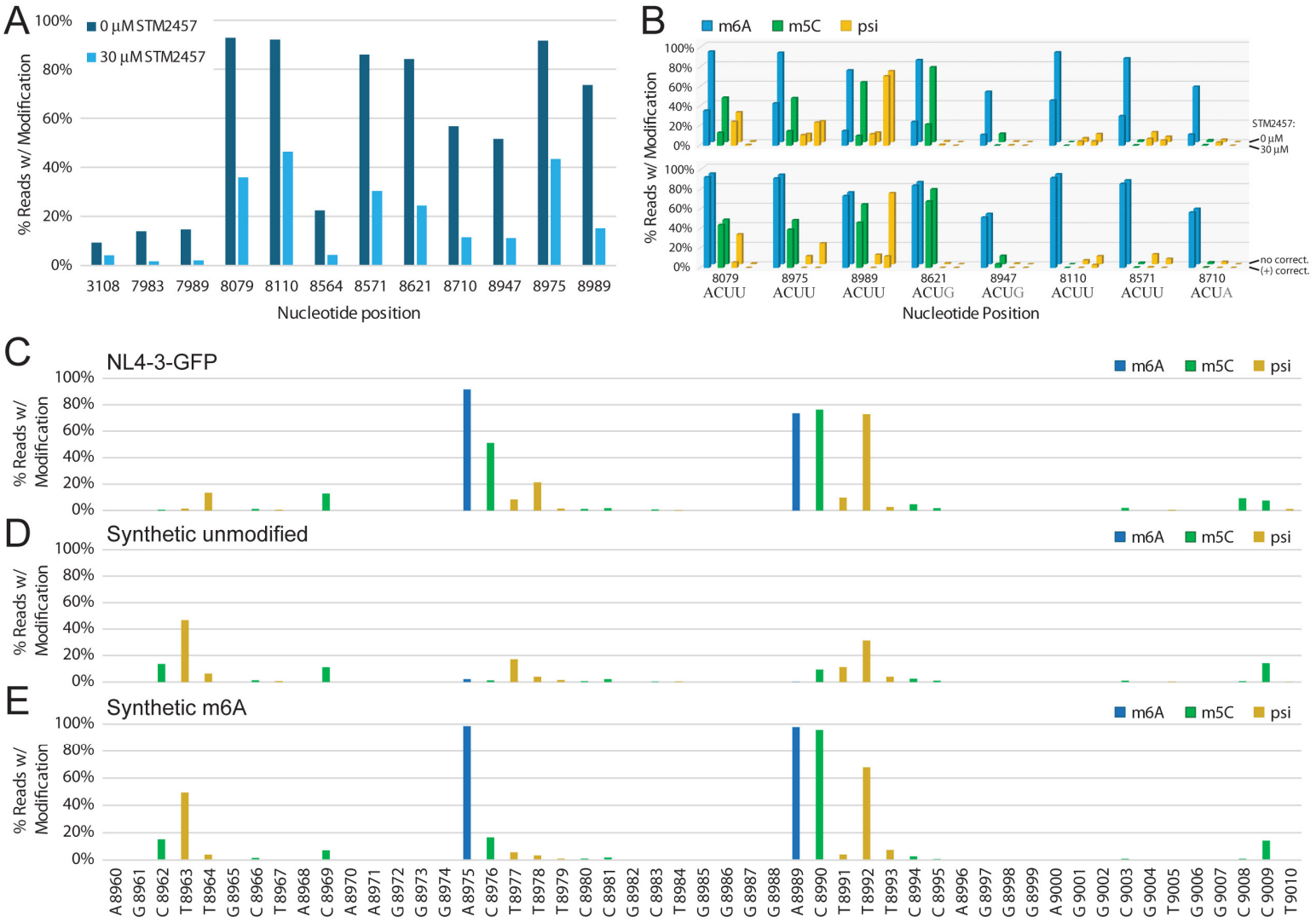

Figure 1. **Probing and correction of HIV-1 base modifications called by nanopore direct RNA sequencing.** (**A**) Nanopore modification-calling results for HIV-1 viral RNA extracted from Jurkat cell cultures treated with STM2457, a drug that inhibits METTL3 m^{6}A modification activity. The position of each high frequency m^{6}A nucleotide in the HIV-1 genome is indicated on the x-axis. (**B**) Comparison of modifications at DRACH motif sites where m^{6}A was called at high frequency. The nucleotide position of the m^{6}A modification within the DRACH motif is indicated on the x-axis. Upper plot: comparison of Jurkat cell samples infected with HIV-1 without (back row) or with (front row) 30 µM STM2457 treatment. Lower graph: comparison of Jurkat cell sample infected with HIV-1 before (front row) and after (back row) baseline correction. (**C-E**) Comparison of modification calling between NL4-3 from Jurkat cells (C) and two synthetic HIV-1 RNA fragments, one unmodified (D) and one bearing m^{6}A (E) at two DRACH motifs. The nucleotide position corresponding to the NL4-3 genome is indicated on the x-axis. All modifications called in panel D are incorrect while modifications called in panel E, besides m^{6}A at position 8975 and 8989, are incorrect.

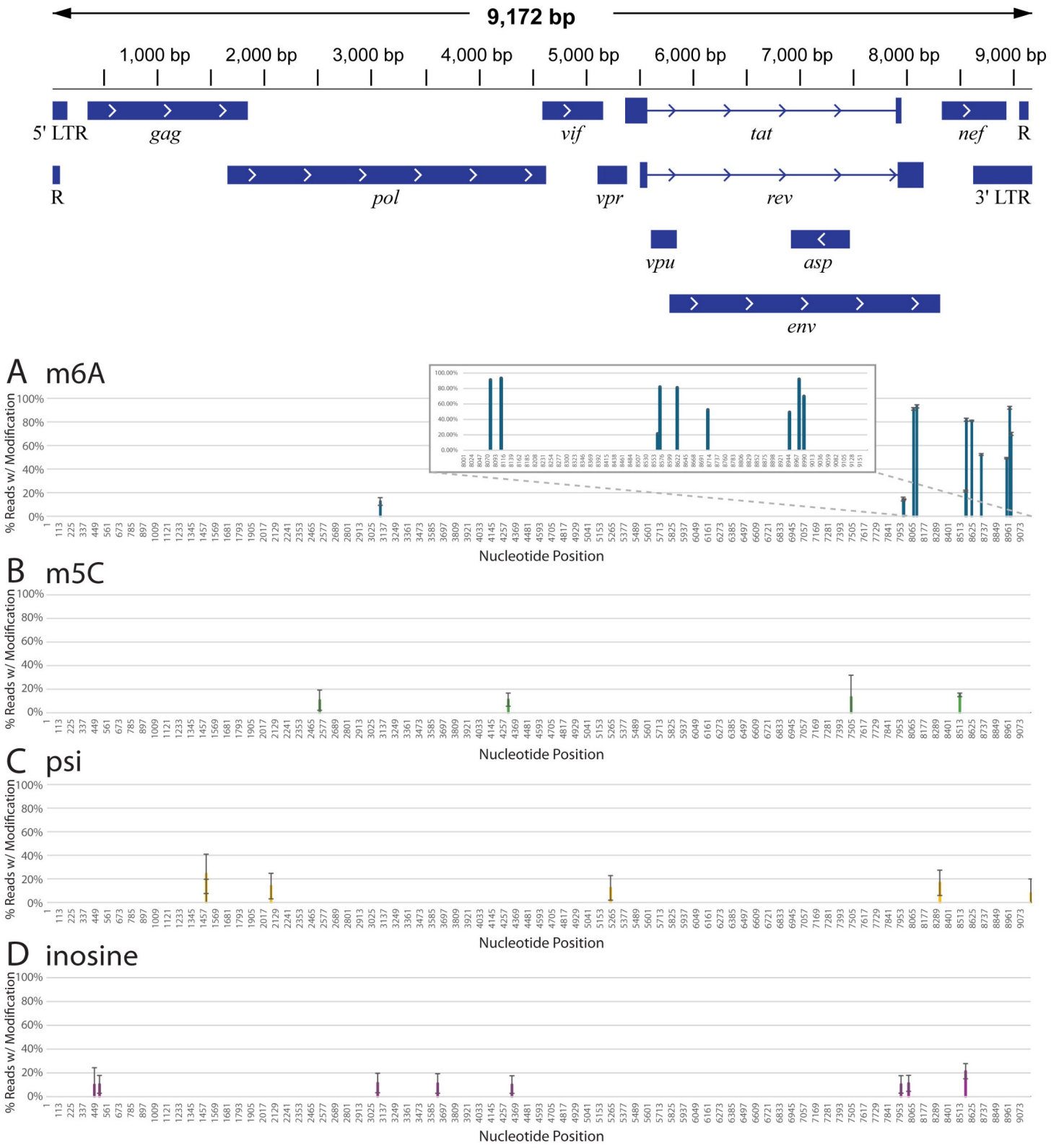

Figure 2. **Corrected nanopore modification calling results for HIV-1 viral RNA from Jurkat cells**. The HIV-1 genome architecture is illustrated above. m^{6}A (blue), m^{5}C (green), pseudouridine (psi) (yellow), and inosine (purple). Inset in panel A is a close-up of the 3' end of the NL4-3 HIV-1 genome where m^{6}A is most densely called. Results are the average of three separate biological replicates. Error bars are standard deviation.

A

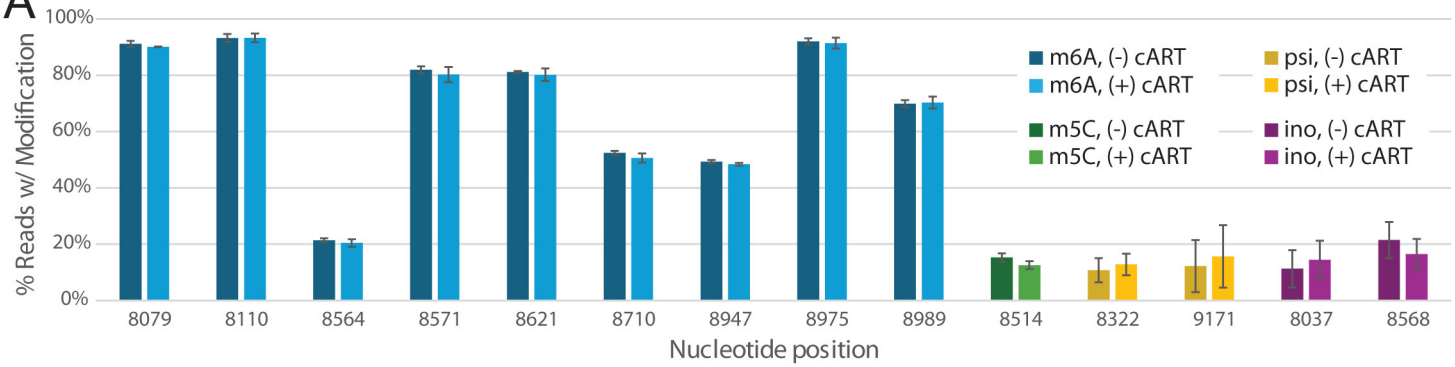

B

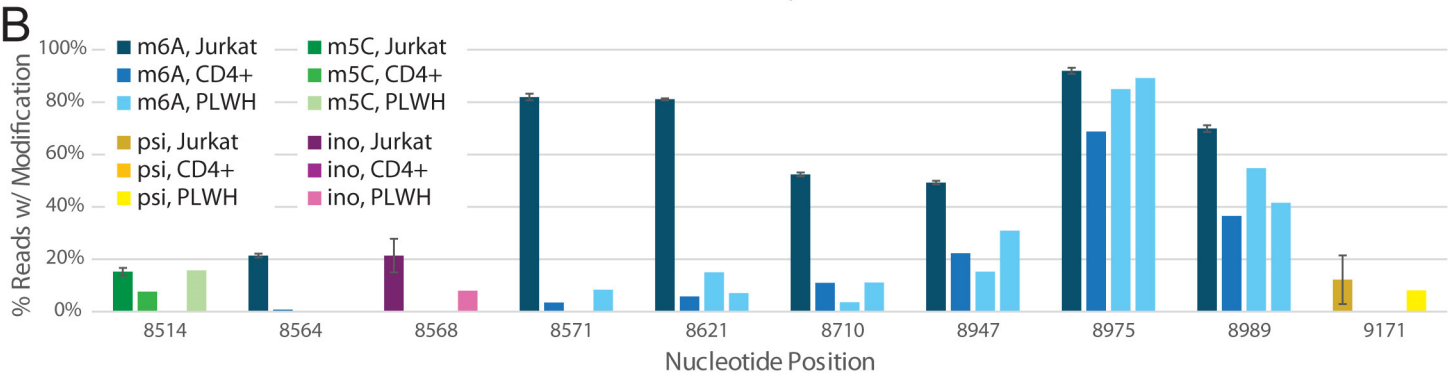

C

Center A of DRACH motif	8079	8110	8179	8199	8237	8305	8440	8450	8485	8564	8571	8621	8651	8710	8745	8815	8857	8890	8947	8954	8975	8989	9018	9092	9123	9131
Jurkat m^{6}A average	91%	93%	12%	11%	12%	3%	12%	7%	4%	21%	82%	81%	4%	52%	10%	7%	2%	4%	49%	2%	92%	70%	8%	0%	0%	5%
DRACH preserved PLWH 5?	Yes	Yes	Yes	No	Yes	Yes	Yes	Yes	No	Yes	Yes	Yes	Yes	Yes	Yes	Yes	Yes	Yes	Yes	Yes	Yes	Yes	Yes	Yes	No	Yes
DRACH preserved PLWH 6?	Yes	Yes	Yes	No	Yes	Yes	Yes	Yes	No	Yes	Yes	Yes	No	Yes	Yes	No	Yes	Yes	Yes	No	Yes	Yes	Yes	Yes	Yes	Yes

HIV-1 mutations (events), Nextclade (HXB2)	Average	Median
Max events per NT found:	406	
Average events per NT: (full genome)	48.17	27
Events per NT: (nucleotides 8000-9171)	50.98	32
Events for m6A sites: (nucleotides 8000-9171)	**16.38**	**9**

D

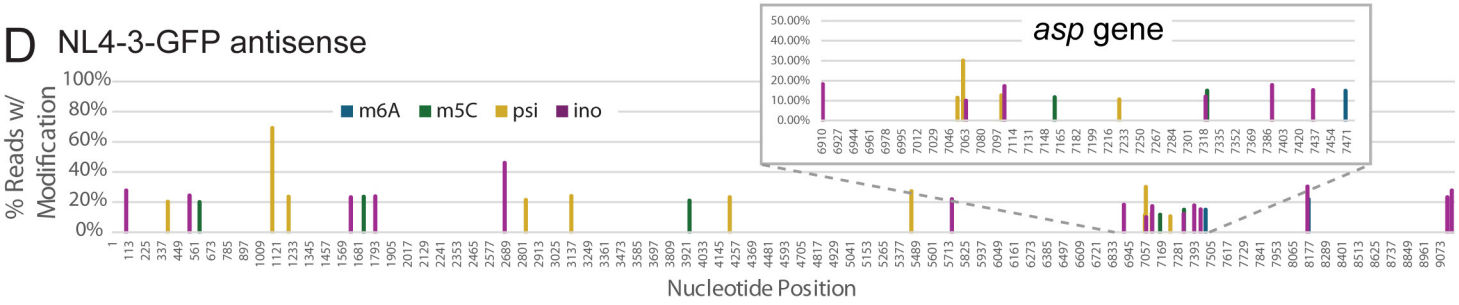

Figure 3. Effect of cART and cell type on HIV-1 modification calling, conservation of m^{6}A in HIV-1 genomes from PLWH samples, and a preliminary HIV-1 antisense epitranscriptome. (**A**) Nanopore modification-calling results for HIV-1 RNA taken from Jurkats treated without (darker color) or with (lighter color) cART treatment. Error bars represent the standard deviation from three separate biological replicates. (**B**) Nanopore modification-calling results for HIV-1 RNA taken from Jurkat, primary CD4+ T cells infected *in vitro*, and CD4+ T cells from PLWH samples. In each nucleotide position cluster, the first column is Jurkat cell samples infected with HIV-1, the second column is CD4+ T cells from healthy donors and infected with HIV-1, and the third and fourth columns are samples taken from CD4+ T cells from PLWH donors. (**C**) Top: comparison of m^{6}A modifications called from HIV-1 RNA from Jurkat cells against preservation of the DRACH motifs for these m^{6}A modifications sequenced from two PLWH samples. Bottom: analysis of preservation of known m^{6}A modification sites in a larger dataset of HIV-1 mutations. Positions containing m^{6}A between nucleotide positions 8000 and 9171 were identified and the average and median events for these positions are shown. (**D**) Antisense nanopore modification-calling for HIV-1 viral RNA from Jurkat cells. m6A (blue), m5C (green), pseudouridine (yellow), and inosine (purple). Inset shows a close-up of the *asp* gene.

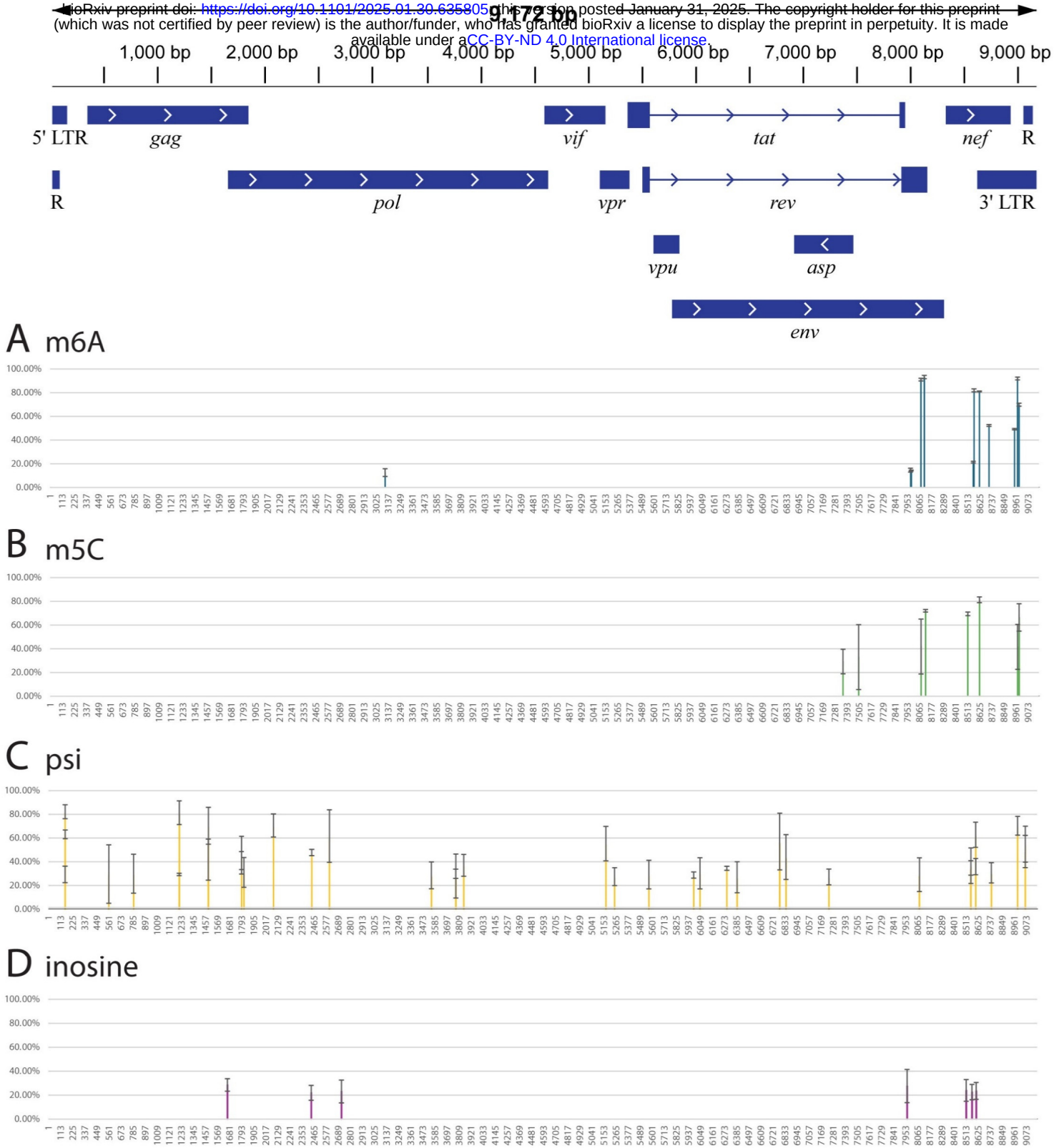

Figure S1. **Uncorrected nanopore modification-calling results for HIV-1 viral RNA from Jurkat cells**. X-axis represents individual nucleotides in the HIV-1 genome. Y-axis represents percentage of reads that contained the mutation of interest for that nucleotide. m^6A (blue), m^5C (green), pseudouridine (psi) (yellow), and inosine (purple). Results are the average of three separate biological replicates. Error bars are standard deviation.

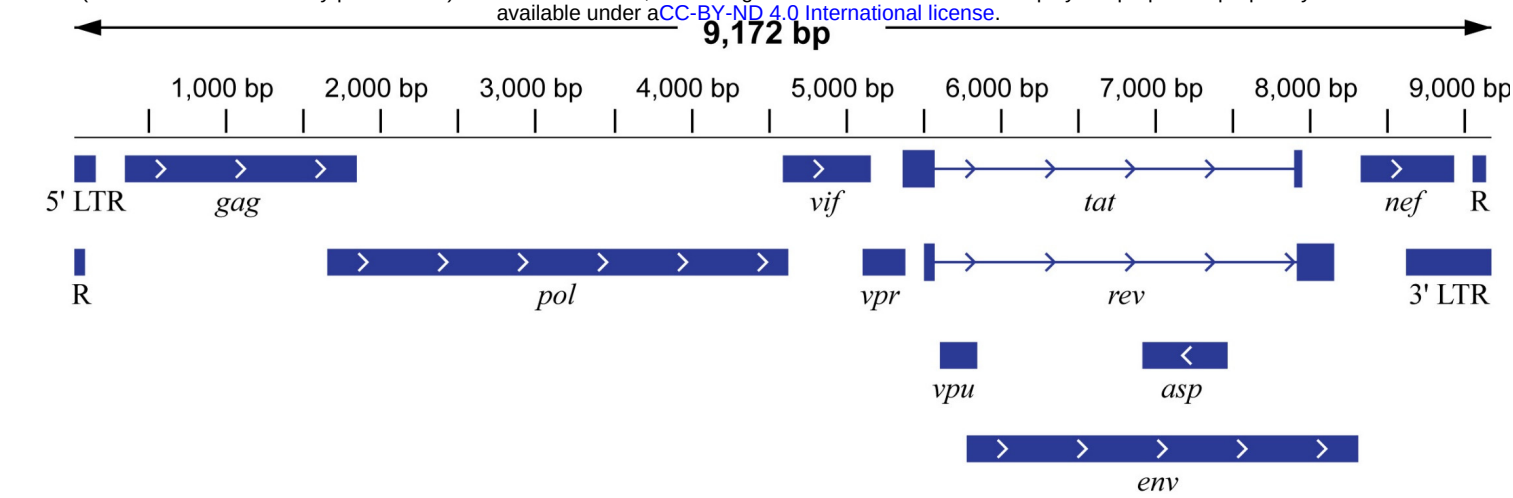

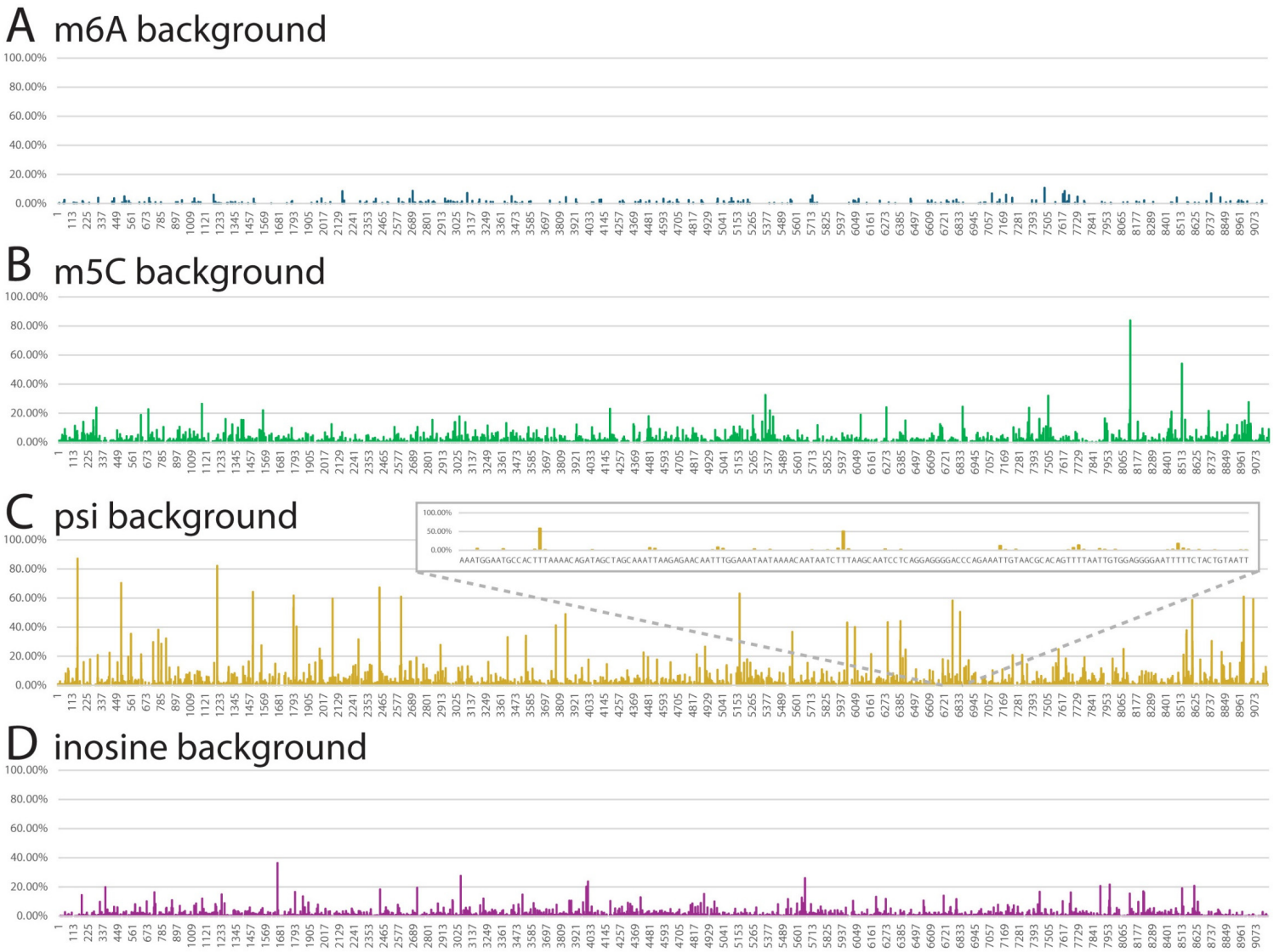

Figure S2. Modification calling from nanopore sequencing of *in vitro* transcribed NL4-3 HIV-1 RNA fragments used for baseline correction. X-axis represents individual nucleotides in the HIV-1 genome. Y-axis represents percentage of reads that contained the mutation of interest for that nucleotide. m^6A (blue), m^5C (green), pseudouridine (psi) (yellow), and inosine (purple).

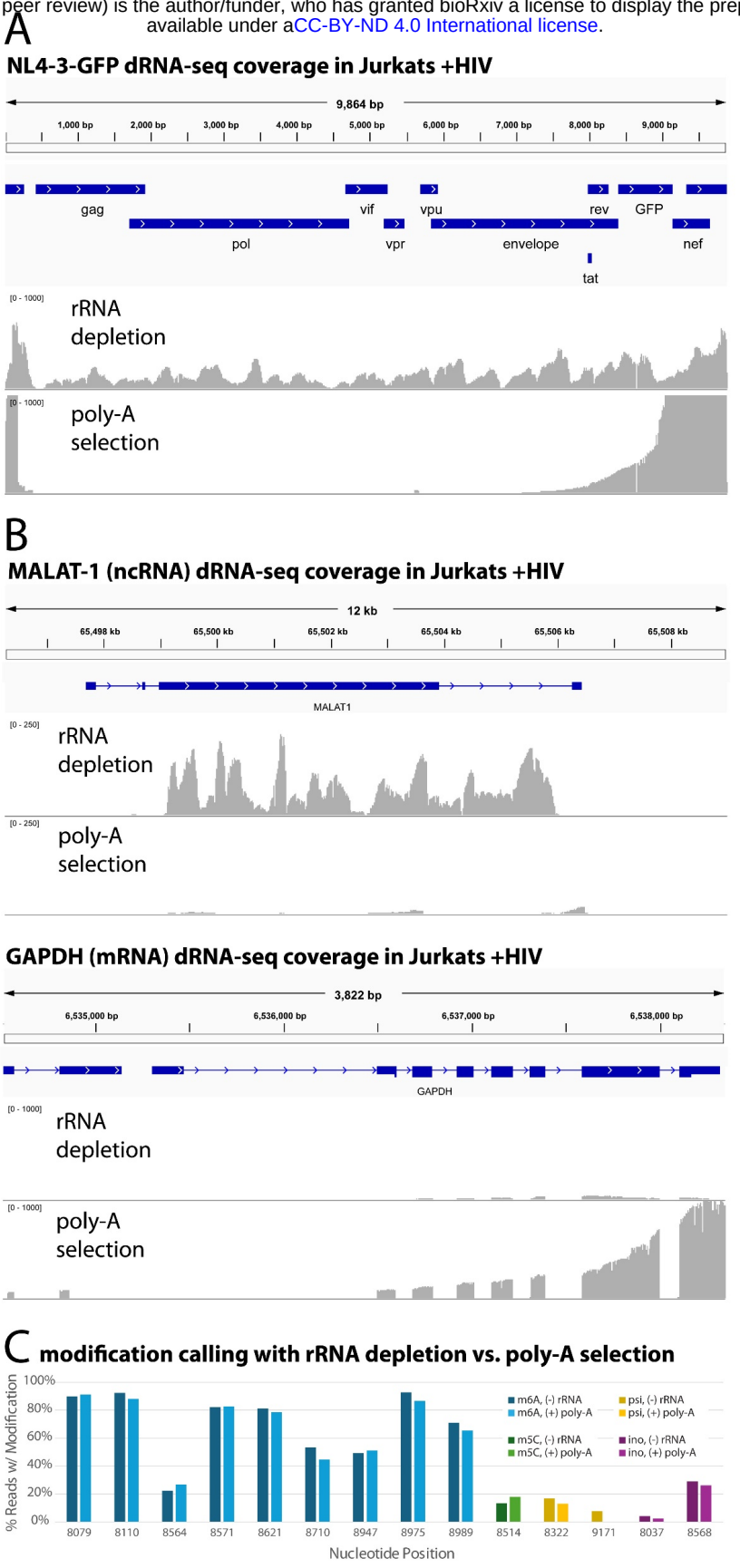

Figure S3. **Comparison of rRNA depletion and poly-A selection using read coverage maps and modified base calling from nanopore dRNA-seq**. X-axis is the individual nucleotide positions. Y-axis is the number of reads with coverage at that position. Samples are from Jurkat cells infected with NL4-3-GFP HIV-1. (**A**) Comparison of HIV-1 sequencing coverage from rRNA depletion or poly-A selection. (**B**) Comparison of human noncoding RNA MALAT-1 and mRNA GAPDH sequencing coverage for each RNA preparation method. (**C**) Modification calling results for HIV-1 viral RNA taken from Jurkat cell cultures and rRNA deplated or poly-A selected prior to dRNA-seq. m^6A (blue), m^5C (green), pseudouridine (psi) (yellow), and inosine (purple).

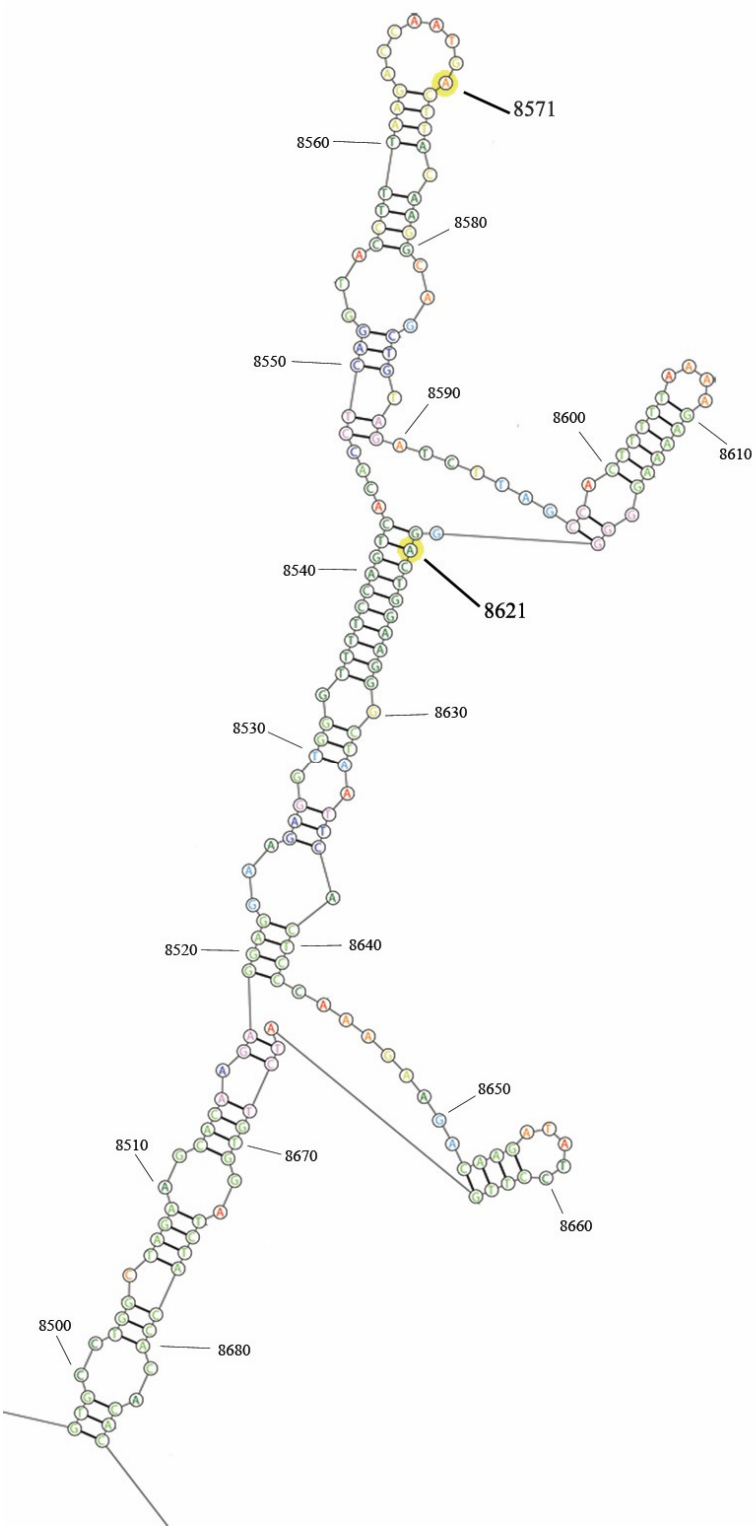

Figure S4. Folding model of the HIV-1 RNA region surrounding two potential m^{6}A modification nucleotide positions in *nef* gene. Folding model generated via the RNAstructure program (https://rna.urmc.rochester.edu/RNAstructure.html). m^{6}A modification positions (8571, 8621) are labeled and indicated in yellow.

Table S1. Significant m6A modification sites in HIV-1 epitranscriptome.

	Jurkat cells with HIV-GFPΔEnv/VSV-G					Jurkat cells with HIV-GFPΔEnv/VSV-G and cART					Jurkats cells (ribosome depletion method)		CD4 T-cells with NL4-3 HIV	Patient CD4 T-cells		m6A Chemical Knockdown	
Base	7C	11E	11B/H	HIV average	HIV stdev	7E	11F	11C/I	HIV+cART average	HIV+cART stdev	Poly-A-selection	RNaseH reaction	10D	P5S2	P6S	STM2457 0 μM	STM2457 30 μM
3108	16.08%	8.33%	13.33%	12.58%	±3.21%	12.41%	7.14%	7.69%	9.08%	±2.37%	-	-	25.00%	-	-	9.30%	4.17%
7983	13.22%	16.92%	13.69%	14.61%	±1.64%	13.36%	11.65%	13.60%	12.87%	±0.87%	13.86%	18.92%	4.89%	-	-	13.91%	1.73%
7989	14.25%	14.81%	14.10%	14.39%	±0.31%	14.70%	11.73%	14.52%	13.65%	±1.36%	14.13%	11.54%	4.92%	-	-	14.71%	2.05%
8079	91.02%	92.49%	89.77%	91.09%	±1.11%	89.94%	90.30%	89.99%	90.08%	±0.16%	89.82%	91.07%	55.68%	-	-	92.83%	35.93%
8110	95.19%	92.24%	92.24%	93.22%	±1.39%	93.99%	91.16%	94.65%	93.26%	±1.51%	92.39%	88.24%	57.35%	-	-	92.03%	46.36%
8564	20.76%	21.06%	22.40%	21.41%	±0.71%	18.54%	21.56%	21.22%	20.44%	±1.35%	22.47%	26.83%	0.79%	0.00%	0.00%	22.43%	4.27%
8571	80.22%	83.25%	82.36%	81.94%	±1.27%	76.48%	82.56%	81.71%	80.25%	±2.69%	82.28%	82.76%	3.51%	0.00%	8.33%	85.93%	30.35%
8621	81.11%	80.62%	81.53%	81.09%	±0.37%	76.95%	81.98%	81.53%	80.15%	±2.27%	81.23%	78.72%	5.78%	15.00%	7.14%	84.13%	24.41%
8710	52.35%	51.54%	53.33%	52.41%	±0.73%	48.45%	51.17%	52.20%	50.61%	±1.58%	53.32%	44.62%	11.00%	3.57%	11.11%	56.72%	11.50%
8947	50.04%	48.45%	49.31%	49.27%	±0.65%	47.74%	48.88%	48.47%	48.36%	±0.47%	49.29%	51.25%	22.29%	15.25%	30.95%	51.58%	11.16%
8975	90.36%	92.84%	92.76%	91.99%	±1.15%	88.77%	93.44%	91.98%	91.40%	±1.95%	92.77%	86.67%	68.74%	85.00%	89.13%	91.60%	43.39%
8989	68.09%	70.65%	70.96%	69.90%	±1.28%	67.38%	72.14%	71.33%	70.29%	±2.08%	71.09%	65.42%	36.57%	54.84%	41.54%	73.56%	15.15%

Table S2. Significant m5C modification sites in HIV-1 epitranscriptome.

		Jurkat cells with HIV-GFPΔEnv/VSV-G						Jurkat cells with HIV-GFPΔEnv/VSV-G and cART					(ribosome depletion method) 11B/H		CD4 T-cells with NL4-3 HIV	Patient CD4 T-cells		m6A Chemical Knockdown	
Base	T7-InVitro	7C minus T7	11E minus T7	11B/H minus T7	HIV average	HIV stdev	m6A Adjacent ?	7E minus T7	11F minus T7	11C/I minus T7	HIV+cART average	HIV+cART stdev	Poly-A-selection minus T7	RNaseH reaction minus T7	10D minus T7	P5S2 minus T7	P6S minus T7	STM2457 0 μM minus T7	STM2457 30 μM minus T7
2547	10.60%	5.73%	22.73%	3.68%	10.72%	±8.54%	No	0.40%	0.00%	0.00%	0.13%	±0.19%	-	9.40%	0.00%	-	-	0.33%	0.00%
4305	0.78%	13.02%	16.86%	3.66%	11.18%	±5.54%	No	9.60%	4.88%	0.00%	4.82%	±3.92%	4.77%	-	0.00%	-	-	1.37%	1.85%
7501	32.06%	39.66%	0.00%	0.00%	13.22%	±18.70%	No	39.31%	0.00%	0.00%	13.10%	±18.53%	0.00%	0.00%	0.00%	-	-	0.00%	0.00%
8080	1.70%	8.29%	49.97%	62.49%	40.25%	±23.17%	Yes	10.30%	25.13%	52.67%	29.37%	±17.56%	63.50%	20.80%	25.58%	-	-	45.52%	13.35%
8514	54.22%	15.02%	17.14%	13.57%	15.24%	±1.47%	No	14.52%	11.15%	11.99%	12.55%	±1.43%	13.44%	18.01%	7.59%	-	15.78%	8.47%	6.26%
8622	8.71%	69.48%	72.88%	75.48%	72.61%	±2.46%	Yes	66.78%	73.47%	74.55%	71.60%	±3.44%	75.17%	72.69%	4.73%	14.82%	0.00%	76.74%	21.81%
8976	6.03%	8.80%	49.32%	48.59%	35.57%	±18.93%	Yes	9.90%	35.88%	48.25%	31.34%	±15.98%	48.91%	39.25%	31.76%	50.38%	22.54%	45.12%	14.97%
8990	15.05%	35.16%	58.32%	60.81%	51.43%	±11.55%	Yes	36.20%	56.73%	60.68%	51.20%	±10.73%	60.98%	47.31%	31.49%	40.71%	24.23%	61.31%	10.18%

Table S3. Significant pseudouridine (psi) modification sites in HIV-1 epitranscriptome.

		Jurkat cells with HIV-GFPΔEnv/VSV-G					Jurkat cells with HIV-GFPΔEnv/VSV-G and cART					Jurkats cells (ribosome depletion method)		CD4 T-cells with NL4-3 HIV	Patient CD4 T-cells		m6A Chemical Knockdown	
Base	T7-InVitro	7C minus T7	11E minus T7	11B/H minus T7	HIV average 7C,11B,11E,11H	HIV stdev	7E minus T7	11F minus T7	11C/I minus T7	HIV+cART average 7E,11C,11F,11I	HIV+cART stdev	Poly-A-selection minus T7	RNaseH reaction minus T7	10D minus T7	P5S2 minus T7	P6S minus T7	STM2457 0 μM minus T7	STM2457 30 μM minus T7
1483	27.51%	0.00%	25.82%	24.34%	16.72%	±11.84%	0.00%	6.70%	9.33%	5.34%	±3.93%	-	14.59%	17.94%	-	-	1.33%	0.00%
1484	64.29%	0.00%	20.71%	9.63%	10.11%	±8.46%	0.00%	9.71%	21.43%	10.38%	±8.76%	-	22.38%	-	-	-	9.05%	17.25%
2088	59.72%	0.00%	18.54%	13.96%	10.83%	±7.89%	0.00%	0.00%	0.00%	0.00%	±0.00%	0.28%	-	16.75%	-	-	4.34%	8.07%
5253	15.57%	0.38%	18.47%	12.40%	10.42%	±7.52%	1.24%	11.41%	0.00%	4.22%	±5.11%	10.79%	23.32%	10.22%	-	-	16.54%	5.72%
8322	1.96%	8.17%	7.27%	16.76%	10.73%	±4.28%	7.70%	13.75%	16.94%	12.80%	±3.83%	16.87%	13.04%	0.00%	0.00%	-	14.50%	1.15%
9171	0.82%	25.14%	3.84%	7.68%	12.22%	±9.27%	31.29%	8.33%	7.33%	15.65%	±11.06%	7.66%	0.00%	0.21%	0.00%	8.06%	14.45%	13.48%

Table S4. Significant inosine modification sites in HIV-1 epitranscriptome.

		Jurkat cells with HIV-GFPΔEnv/VSV-G					Jurkat cells with HIV-GFPΔEnv/VSV-G and cART					Jurkats cells (ribosome depletion method)		CD4 T-cells with NL4-3 HIV	Patient CD4 T-cells		m6A Chemical Knockdown	
Base	T7-InVitro	7C minus T7	11E minus T7	11B/H minus T7	HIV average 7C,11E,11B/H	HIV stdev	7E minus T7	11F minus T7	11C/I minus T7	HIV+cART average	HIV+cART stdev	Poly-A-selection minus T7	RNaseH reaction minus T7	10D minus T7	P5S2 minus T7	P6S minus T7	STM2457 0 μM minus T7	STM2457 30 μM minus T7
448	6.09%	0.00%	0.00%	30.28%	10.09%	±14.27%	4.44%	3.91%	0.00%	4.18%	±0.26%	-	-	0.00%	-	-	18.91%	0.00%
495	2.82%	0.00%	13.85%	17.18%	10.34%	±7.44%	0.00%	1.62%	0.00%	0.81%	±0.81%	-	-	4.32%	-	-	4.08%	0.00%
3088	5.73%	0.00%	16.49%	18.07%	11.52%	±8.17%	0.00%	1.81%	0.00%	0.91%	±0.91%	-	32.73%	0.00%	-	-	1.28%	0.72%
3647	3.81%	0.00%	13.97%	19.45%	11.14%	±8.19%	0.00%	8.92%	15.24%	4.46%	±4.46%	16.19%	22.28%	8.10%	-	-	23.67%	7.19%
4340	5.65%	0.00%	13.10%	17.42%	10.17%	±7.41%	0.00%	0.01%	0.80%	0.00%	±0.00%	14.86%	25.12%	9.87%	-	-	4.35%	3.32%
7966	21.75%	0.00%	15.85%	15.38%	10.41%	±7.36%	0.00%	0.00%	8.72%	0.00%	±0.00%	15.60%	16.89%	7.75%	-	-	22.43%	9.71%
8037	4.51%	20.09%	9.64%	4.05%	11.26%	±6.65%	21.23%	7.61%	4.26%	14.42%	±6.81%	4.13%	2.46%	1.17%	-	-	8.75%	0.00%
8568	1.09%	13.69%	21.26%	29.40%	21.45%	±6.42%	11.14%	21.87%	26.53%	16.51%	±5.36%	29.04%	26.18%	0.00%	0.00%	8.00%	28.15%	6.52%

Table S5. Significant modification sites in the NL4-3-GFP HIV-1 antisense epitranscriptome.

Whole genome, mod% > 20%, at least 10x coverage

		m6A			m5C			Pseudouridine			Inosine		
	Base	Jurkats	T7	Diff	Jurkats	T7	Diff	Jurkats	T7	Diff	Jurkats	T7	Diff
A	46	0.00%	0.00%	0.00%	0.00%	0.00%	0.00%	0.00%	0.00%	0.00%	40.00%	6.60%	33.40%
A	95	0.00%	0.00%	0.00%	0.00%	0.00%	0.00%	0.00%	0.00%	0.00%	30.00%	2.27%	27.73%
T	379	0.00%	0.00%	0.00%	0.00%	0.00%	0.00%	25.00%	4.76%	20.24%	0.00%	0.00%	0.00%
A	527	0.00%	0.00%	0.00%	0.00%	0.00%	0.00%	0.00%	0.00%	0.00%	50.00%	25.53%	24.47%
C	596	0.00%	0.00%	0.00%	20.00%	0.00%	20.00%	0.00%	0.00%	0.00%	0.00%	0.00%	0.00%
T	1093	0.00%	0.00%	0.00%	0.00%	0.00%	0.00%	69.23%	0.00%	69.23%	0.00%	0.00%	0.00%
T	1204	0.00%	0.00%	0.00%	0.00%	0.00%	0.00%	27.27%	3.64%	23.64%	0.00%	0.00%	0.00%
A	1629	0.00%	0.00%	0.00%	0.00%	0.00%	0.00%	0.00%	0.00%	0.00%	27.27%	4.00%	23.27%
C	1717	0.00%	0.00%	0.00%	40.00%	16.36%	23.64%	0.00%	0.00%	0.00%	0.00%	0.00%	0.00%
A	1797	0.00%	0.00%	0.00%	0.00%	0.00%	0.00%	0.00%	0.00%	0.00%	27.27%	3.49%	23.78%
A	2680	0.00%	0.00%	0.00%	0.00%	0.00%	0.00%	0.00%	0.00%	0.00%	60.00%	14.00%	46.00%
T	2826	0.00%	0.00%	0.00%	0.00%	0.00%	0.00%	25.00%	3.58%	21.42%	0.00%	0.00%	0.00%
T	3136	0.00%	0.00%	0.00%	0.00%	0.00%	0.00%	27.27%	3.21%	24.07%	0.00%	0.00%	0.00%
C	3943	0.00%	0.00%	0.00%	21.43%	0.45%	20.98%	0.00%	0.00%	0.00%	0.00%	0.00%	0.00%
T	4219	0.00%	0.00%	0.00%	0.00%	0.00%	0.00%	27.27%	4.05%	23.23%	0.00%	0.00%	0.00%
T	5459	0.00%	0.00%	0.00%	0.00%	0.00%	0.00%	40.00%	12.76%	27.24%	0.00%	0.00%	0.00%
A	5736	0.00%	0.00%	0.00%	0.00%	0.00%	0.00%	0.00%	0.00%	0.00%	27.27%	5.34%	21.93%
T	7061	0.00%	0.00%	0.00%	0.00%	0.00%	0.00%	46.43%	16.29%	30.14%	0.00%	0.00%	0.00%
A	8165	0.00%	0.00%	0.00%	0.00%	0.00%	0.00%	0.00%	0.00%	0.00%	30.77%	0.48%	30.29%
A	8173	23.53%	1.65%	21.88%	0.00%	0.00%	0.00%	0.00%	0.00%	0.00%	0.00%	0.00%	0.00%
A	9121	0.00%	0.00%	0.00%	0.00%	0.00%	0.00%	0.00%	0.00%	0.00%	30.77%	7.55%	23.22%
A	9151	0.00%	0.00%	0.00%	0.00%	0.00%	0.00%	0.00%	0.00%	0.00%	35.71%	8.03%	27.68%

ASP gene only, mod% > 10%

		m6A			m5C			Pseudouridine			Inosine		
	Base	Jurkats	T7	Diff	Jurkats	T7	Diff	Jurkats	T7	Diff	Jurkats	T7	Diff
A	6911	0.00%	0.00%	0.00%	0.00%	0.00%	0.00%	0.00%	0.00%	0.00%	18.52%	0.27%	18.25%
T	7055	0.00%	0.00%	0.00%	0.00%	0.00%	0.00%	21.21%	9.74%	11.47%	0.00%	0.00%	0.00%
T	7061	0.00%	0.00%	0.00%	0.00%	0.00%	0.00%	46.43%	16.29%	30.14%	0.00%	0.00%	0.00%
A	7064	0.00%	0.00%	0.00%	0.00%	0.00%	0.00%	0.00%	0.00%	0.00%	10.00%	0.00%	10.00%
T	7102	0.00%	0.00%	0.00%	0.00%	0.00%	0.00%	40.54%	27.92%	12.62%	0.00%	0.00%	0.00%
A	7105	0.00%	0.00%	0.00%	0.00%	0.00%	0.00%	0.00%	0.00%	0.00%	18.42%	1.15%	17.27%
C	7159	0.00%	0.00%	0.00%	40.74%	29.08%	11.66%	0.00%	0.00%	0.00%	0.00%	0.00%	0.00%
T	7228	0.00%	0.00%	0.00%	0.00%	0.00%	0.00%	23.08%	12.50%	10.58%	0.00%	0.00%	0.00%
A	7320	0.00%	0.00%	0.00%	0.00%	0.00%	0.00%	0.00%	0.00%	0.00%	18.52%	6.45%	12.07%
C	7322	0.00%	0.00%	0.00%	19.35%	4.39%	14.97%	0.00%	0.00%	0.00%	0.00%	0.00%	0.00%
A	7391	0.00%	0.00%	0.00%	0.00%	0.00%	0.00%	0.00%	0.00%	0.00%	31.25%	13.40%	17.85%
A	7435	0.00%	0.00%	0.00%	0.00%	0.00%	0.00%	0.00%	0.00%	0.00%	20.00%	4.76%	15.24%
A	7470	18.92%	4.00%	14.92%	0.00%	0.00%	0.00%	0.00%	0.00%	0.00%	0.00%	0.00%	0.00%

REFERENCES

Abudayyeh, O.O., Gootenberg, J.S., Franklin, B., Koob, J., Kellner, M.J., Ladha, A., Joung, J., Kirchgatterer, P., Cox, D.B.T., and Zhang, F. (2019). A cytosine deaminase for programmable single-base RNA editing. Science *365*, 382-386.

Ageely, E.A., Chilamkurthy, R., Jana, S., Abdullahu, L., O'Reilly, D., Jensik, P.J., Damha, M.J., and Gagnon, K.T. (2021). Gene editing with CRISPR-Cas12a guides possessing ribose-modified pseudoknot handles. Nature communications *12*, 6591.

Aksamentov, I., Roemer, C., Hodcroft, E., and Neher, R. (2021). Nextclade: clade assignment, mutation calling and quality control for viral genomes. Journal of Open Source Software *6*, 3773.

Baek, A., Lee, G.E., Golconda, S., Rayhan, A., Manganaris, A.A., Chen, S., Tirumuru, N., Yu, H., Kim, S., Kimmel, C.*, et al.* (2024). Single-molecule epitranscriptomic analysis of full-length HIV-1 RNAs reveals functional roles of site-specific m(6)As. Nature microbiology *9*, 1340-1355.

Baldwin, A., Morris, A.R., and Mukherjee, N. (2021). An Easy, Cost-Effective, and Scalable Method to Deplete Human Ribosomal RNA for RNA-seq. Current protocols *1*, e176.

Best, B.M., Koopmans, P.P., Letendre, S.L., Capparelli, E.V., Rossi, S.S., Clifford, D.B., Collier, A.C., Gelman, B.B., Mbeo, G., McCutchan, J.A.*, et al.* (2011). Efavirenz concentrations in CSF exceed IC50 for wild-type HIV. The Journal of antimicrobial chemotherapy *66*, 354-357.

Boccaletto, P., Stefaniak, F., Ray, A., Cappannini, A., Mukherjee, S., Purta, E., Kurkowska, M., Shirvanizadeh, N., Destefanis, E., Groza, P.*, et al.* (2022). MODOMICS: a database of RNA modification pathways. 2021 update. Nucleic acids research *50*, D231-D235.

Braddock, M., Thorburn, A.M., Kingsman, A.J., and Kingsman, S.M. (1991). Blocking of Tat-dependent HIV-1 RNA modification by an inhibitor of RNA polymerase II processivity. Nature *350*, 439-441.

Cai, Z., Song, P., Yu, K., and Jia, G. (2024). Advanced reactivity-based sequencing methods for mRNA epitranscriptome profiling. RSC chemical biology.

Cerneckis, J., Ming, G.L., Song, H., He, C., and Shi, Y. (2024). The rise of epitranscriptomics: recent developments and future directions. Trends in pharmacological sciences *45*, 24-38.

Chen, G., Katrekar, D., and Mali, P. (2019). RNA-Guided Adenosine Deaminases: Advances and Challenges for Therapeutic RNA Editing. Biochemistry *58*, 1947-1957.

Chen, S., Kumar, S., Espada, C.E., Tirumuru, N., Cahill, M.P., Hu, L., He, C., and Wu, L. (2021). N6-methyladenosine modification of HIV-1 RNA suppresses type-I interferon induction in differentiated monocytic cells and primary macrophages. PLoS pathogens *17*, e1009421.

Courtney, D.G. (2021). Post-Transcriptional Regulation of Viral RNA through Epitranscriptional Modification. Cells *10*.

Courtney, D.G., Tsai, K., Bogerd, H.P., Kennedy, E.M., Law, B.A., Emery, A., Swanstrom, R., Holley, C.L., and Cullen, B.R. (2019). Epitranscriptomic Addition of m(5)C to HIV-1 Transcripts Regulates Viral Gene Expression. Cell host & microbe *26*, 217-227 e216.

Cox, D.B.T., Gootenberg, J.S., Abudayyeh, O.O., Franklin, B., Kellner, M.J., Joung, J., and Zhang, F. (2017). RNA editing with CRISPR-Cas13. Science *358*, 1019-1027.

Cristinelli, S., Angelino, P., Janowczyk, A., Delorenzi, M., and Ciuffi, A. (2021). HIV Modifies the m6A and m5C Epitranscriptomic Landscape of the Host Cell. Frontiers in Virology *1*.

Dunin-Horkawicz, S., Czerwoniec, A., Gajda, M.J., Feder, M., Grosjean, H., and Bujnicki, J.M. (2006). MODOMICS: a database of RNA modification pathways. Nucleic acids research *34*, D145-149.

Estevez, M., Li, R., Paul, B., Daneshvar, K., Mullen, A.C., Romerio, F., and Addepalli, B. (2022). Identification and mapping of post-transcriptional modifications on the HIV-1 antisense transcript Ast in human cells. RNA *28*, 697-710.

Gao, K., Yang, X., Zhao, W., Lin, Y., Hu, B., and Wang, D. (2025). NAT10 promotes pyroptosis and pancreatic injury of severe acute pancreatitis through ac4C modification of NLRP3. Shock.

Honeycutt, E., Kizito, F., Karn, J., and Sweet, T. (2024). Direct Analysis of HIV mRNA m(6)A Methylation by Nanopore Sequencing. Methods Mol Biol *2807*, 209-227.

Huang, A., Riepler, L., Rieder, D., Kimpel, J., and Lusser, A. (2023). No evidence for epitranscriptomic m(5)C modification of SARS-CoV-2, HIV and MLV viral RNA. RNA *29*, 756-763.

Imam, H., Kim, G.W., and Siddiqui, A. (2020). Epitranscriptomic(N6-methyladenosine) Modification of Viral RNA and Virus-Host Interactions. Frontiers in cellular and infection microbiology *10*, 584283.

Jain, M., Abu-Shumays, R., Olsen, H.E., and Akeson, M. (2022). Advances in nanopore direct RNA sequencing. Nature methods *19*, 1160-1164.

Jia, S., Yu, X., Deng, N., Zheng, C., Ju, M., Wang, F., Zhang, Y., Gao, Z., Li, Y., Zhou, H., *et al.* (2025). Deciphering the pseudouridine nucleobase modification in human diseases: From molecular mechanisms to clinical perspectives. Clinical and translational medicine *15*, e70190.

Kartje, Z.J., Janis, H.I., Mukhopadhyay, S., and Gagnon, K.T. (2021). Revisiting T7 RNA polymerase transcription in vitro with the Broccoli RNA aptamer as a simplified real-time fluorescent reporter. The Journal of biological chemistry *296*, 100175.

Kennedy, E.M., Bogerd, H.P., Kornepati, A.V., Kang, D., Ghoshal, D., Marshall, J.B., Poling, B.C., Tsai, K., Gokhale, N.S., Horner, S.M., *et al.* (2016). Posttranscriptional m(6)A

Editing of HIV-1 mRNAs Enhances Viral Gene Expression. Cell host & microbe *19*, 675-685.

Kennedy, E.M., Bogerd, H.P., Kornepati, A.V.R., Kang, D., Ghoshal, D., Marshall, J.B., Poling, B.C., Tsai, K., Gokhale, N.S., Horner, S.M.*, et al.* (2017). Posttranscriptional m(6)A Editing of HIV-1 mRNAs Enhances Viral Gene Expression. Cell Host Microbe *22*, 830.

Lackey, J.G., Mitra, D., Somoza, M.M., Cerrina, F., and Damha, M.J. (2009). Acetal levulinyl ester (ALE) groups for 2'-hydroxyl protection of ribonucleosides in the synthesis of oligoribonucleotides on glass and microarrays. Journal of the American Chemical Society *131*, 8496-8502.

Latifi, N., Mack, A.M., Tellioglu, I., Di Giorgio, S., and Stafforst, T. (2023). Precise and efficient C-to-U RNA base editing with SNAP-CDAR-S. Nucleic acids research *51*, e84.

Letendre, S.L., Mills, A.M., Tashima, K.T., Thomas, D.A., Min, S.S., Chen, S., Song, I.H., Piscitelli, S.C., and extended, I.N.G.s.t. (2014). ING116070: a study of the pharmacokinetics and antiviral activity of dolutegravir in cerebrospinal fluid in HIV-1-infected, antiretroviral therapy-naive subjects. Clinical infectious diseases : an official publication of the Infectious Diseases Society of America *59*, 1032-1037.

Li, W., Huang, Y., Yuan, H., Han, J., Li, Z., Tong, A., Li, Y., Li, H., Liu, Y., Jia, L.*, et al.* (2024). Characterizing transcripts of HIV-1 different substrains using direct RNA sequencing. Heliyon *10*, e39474.

Liang, Z., Ye, H., Ma, J., Wei, Z., Wang, Y., Zhang, Y., Huang, D., Song, B., Meng, J., Rigden, D.J.*, et al.* (2024). m6A-Atlas v2.0: updated resources for unraveling the N6-methyladenosine (m6A) epitranscriptome among multiple species. Nucleic acids research *52*, D194-D202.

Lichinchi, G., Gao, S., Saletore, Y., Gonzalez, G.M., Bansal, V., Wang, Y., Mason, C.E., and Rana, T.M. (2016). Dynamics of the human and viral m(6)A RNA methylomes during HIV-1 infection of T cells. Nature microbiology *1*, 16011.

Mamede, J.I., Cianci, G.C., Anderson, M.R., and Hope, T.J. (2017). Early cytoplasmic uncoating is associated with infectivity of HIV-1. Proceedings of the National Academy of Sciences of the United States of America *114*, E7169-E7178.

Martinez Campos, C., Tsai, K., Courtney, D.G., Bogerd, H.P., Holley, C.L., and Cullen, B.R. (2021). Mapping of pseudouridine residues on cellular and viral transcripts using a novel antibody-based technique. RNA *27*, 1400-1411.

McDowell, J.A., Chittick, G.E., Ravitch, J.R., Polk, R.E., Kerkering, T.M., and Stein, D.S. (1999). Pharmacokinetics of [(14)C]abacavir, a human immunodeficiency virus type 1 (HIV-1) reverse transcriptase inhibitor, administered in a single oral dose to HIV-1-infected adults: a mass balance study. Antimicrobial agents and chemotherapy *43*, 2855-2861.

Mishra, T., Phillips, S., Zhao, Y., Wilms, B., He, C., and Wu, L. (2024). Epitranscriptomic m(6)A modifications during reactivation of HIV-1 latency in CD4(+) T cells. mBio *15*, e0221424.

Mueller, B.U., Lewis, L.L., Yuen, G.J., Farley, M., Keller, A., Church, J.A., Goldsmith, J.C., Venzon, D.J., Rubin, M., Pizzo, P.A.*, et al.* (1998). Serum and cerebrospinal fluid pharmacokinetics of intravenous and oral lamivudine in human immunodeficiency virus-infected children. Antimicrobial agents and chemotherapy *42*, 3187-3192.

Pereira-Montecinos, C., Toro-Ascuy, D., Ananias-Saez, C., Gaete-Argel, A., Rojas-Fuentes, C., Riquelme-Barrios, S., Rojas-Araya, B., Garcia-de-Gracia, F., Aguilera-Cortes, P., Chnaiderman, J.*, et al.* (2022). Epitranscriptomic regulation of HIV-1 full-length RNA packaging. Nucleic acids research *50*, 2302-2318.

Phillips, S., Mishra, T., Huang, S., and Wu, L. (2024). Functional Impacts of Epitranscriptomic m(6)A Modification on HIV-1 Infection. Viruses *16*.

Reautschnig, P., Fruhner, C., Wahn, N., Wiegand, C.P., Kragness, S., Yung, J.F., Hofacker, D.T., Fisk, J., Eidelman, M., Waffenschmidt, N.*, et al.* (2024). Precise in vivo RNA base editing with a wobble-enhanced circular CLUSTER guide RNA. Nature biotechnology.

Ron, K., Kahn, J., Malka-Tunitsky, N., and Sas-Chen, A. (2025). High-throughput detection of RNA modifications at single base resolution. FEBS letters *599*, 19-32.

Roundtree, I.A., Evans, M.E., Pan, T., and He, C. (2017). Dynamic RNA Modifications in Gene Expression Regulation. Cell *169*, 1187-1200.

Schultz, S., Gomard-Henshaw, K., and Muller, M. (2025). RNA Modifications and Their Role in Regulating KSHV Replication and Pathogenic Mechanisms. Journal of medical virology *97*, e70140.

Sharmeen, L., Bass, B., Sonenberg, N., Weintraub, H., and Groudine, M. (1991). Tat-dependent adenosine-to-inosine modification of wild-type transactivation response RNA. Proceedings of the National Academy of Sciences of the United States of America *88*, 8096-8100.

Tang, Y., Chen, K., Song, B., Ma, J., Wu, X., Xu, Q., Wei, Z., Su, J., Liu, G., Rong, R.*, et al.* (2021). m6A-Atlas: a comprehensive knowledgebase for unraveling the N6-methyladenosine (m6A) epitranscriptome. Nucleic acids research *49*, D134-D143.

Tashima, K.T., Caliendo, A.M., Ahmad, M., Gormley, J.M., Fiske, W.D., Brennan, J.M., and Flanigan, T.P. (1999). Cerebrospinal fluid human immunodeficiency virus type 1 (HIV-1) suppression and efavirenz drug concentrations in HIV-1-infected patients receiving combination therapy. The Journal of infectious diseases *180*, 862-864.

Tirumuru, N., Zhao, B.S., Lu, W., Lu, Z., He, C., and Wu, L. (2016). N(6)-methyladenosine of HIV-1 RNA regulates viral infection and HIV-1 Gag protein expression. eLife *5*.

Tsai, K., Bogerd, H.P., Kennedy, E.M., Emery, A., Swanstrom, R., and Cullen, B.R. (2021). Epitranscriptomic addition of m(6)A regulates HIV-1 RNA stability and alternative splicing. Genes & development *35*, 992-1004.

Tsai, K., Jaguva Vasudevan, A.A., Martinez Campos, C., Emery, A., Swanstrom, R., and Cullen, B.R. (2020). Acetylation of Cytidine Residues Boosts HIV-1 Gene Expression by Increasing Viral RNA Stability. Cell host & microbe *28*, 306-312 e306.

van Praag, R.M., van Weert, E.C., van Heeswijk, R.P., Zhou, X.J., Sommadossi, J.P., Jurriaans, S., Lange, J.M., Hoetelmans, R.M., and Prins, J.M. (2002). Stable concentrations of zidovudine, stavudine, lamivudine, abacavir, and nevirapine in serum and cerebrospinal fluid during 2 years of therapy. Antimicrobial agents and chemotherapy *46*, 896-899.

Verhamme, R., and Favoreel, H.W. (2025). The role of N(6)-methyladenosine (m(6)A) mRNA modifications in herpesvirus infections. Journal of virology, e0172324.

Wang, S., Li, H., Lian, Z., and Deng, S. (2022). The Role of RNA Modification in HIV-1 Infection. International journal of molecular sciences *23*.

Wilson, C., Chen, P.J., Miao, Z., and Liu, D.R. (2020). Programmable m(6)A modification of cellular RNAs with a Cas13-directed methyltransferase. Nature biotechnology *38*, 1431-1440.

Xia, Z., Tang, M., Ma, J., Zhang, H., Gimple, R.C., Prager, B.C., Tang, H., Sun, C., Liu, F., Lin, P.*, et al.* (2021). Epitranscriptomic editing of the RNA N6-methyladenosine modification by dCasRx conjugated methyltransferase and demethylase. Nucleic acids research *49*, 7361-7374.

Yan, G., Xu, Y., Xing, X., Chen, S., and Li, F. (2025). NSUN2-Mediated RNA 5-Methylcytosine Modification of PTEN Regulates Cognitive Impairments of Mice with Sleep Deprivation and Autophagy Through PI3K/AKT Signaling. Neuromolecular medicine *27*, 4.

Yankova, E., Blackaby, W., Albertella, M., Rak, J., De Braekeleer, E., Tsagkogeorga, G., Pilka, E.S., Aspris, D., Leggate, D., Hendrick, A.G.*, et al.* (2021). Small-molecule inhibition of METTL3 as a strategy against myeloid leukaemia. Nature *593*, 597-601.

Yeo, J.Y., Goh, G.R., Su, C.T., and Gan, S.K. (2020). The Determination of HIV-1 RT Mutation Rate, Its Possible Allosteric Effects, and Its Implications on Drug Resistance. Viruses *12*.

Zhang, Q., Kang, Y., Wang, S., Gonzalez, G.M., Li, W., Hui, H., Wang, Y., and Rana, T.M. (2021). HIV reprograms host m(6)Am RNA methylome by viral Vpr protein-mediated degradation of PCIF1. Nature communications *12*, 5543.

Zhang, T., Zhao, F., Li, J., Sun, X., Zhang, X., Wang, H., Fan, P., Lai, L., Li, Z., and Sui, T. (2024). Programmable RNA 5-methylcytosine (m5C) modification of cellular RNAs by dCasRx conjugated methyltransferase and demethylase. Nucleic acids research *52*, 2776-2791.